

Extensive spatio-temporal analyses of surface ozone and related meteorological variables in South Korea for 1999–2010

Jihoon Seo,^{1,3} Daeok Youn,^{2*} Jin Young Kim,¹ and Huikyo Lee⁴

¹Green City Technology Institute, Korea Institute of Science and Technology, Seoul,
South Korea

²Department of Earth Science Education, Chungbuk National University, Cheongju, South
Korea

³School of Earth and Environmental Sciences, Seoul National University, Seoul, South
Korea

⁴Jet Propulsion Laboratory, California Institute of Technology, Pasadena, CA, USA

May 19, 2014

*Corresponding author:

Daeok Youn

Department of Earth Science Education

Chungbuk National University, Cheongju, South Korea

Tel: +82-43-261-2738

E-mail: dyoun@chungbuk.ac.kr

1 **Abstract**

2 Spatio-temporal characteristics of surface ozone (O₃) variations over South Korea are
3 investigated with consideration of meteorological factors and time scales based on the
4 Kolmogorov-Zurbenko filter (KZ-filter), using measurement data at 124 air quality
5 monitoring sites and 72 weather stations for the 12-yr period of 1999–2010. In general, O₃
6 levels at coastal cities are high due to dynamic effects of the sea breeze while those at the
7 inland and Seoul Metropolitan Area (SMA) cities are low due to the NO_x titration by local
8 precursor emissions. We examine the meteorological influences on O₃ using a combined
9 analysis of the KZ-filter and linear regressions between O₃ and meteorological variables.
10 We decomposed O₃ time series at each site into short-term, seasonal, and long-term
11 components by the KZ-filter and regressed on meteorological variables. Impact of
12 temperature on the O₃ levels is significantly high in the highly populated SMA and inland
13 region, but low in the coastal region. In particular, the probability of high O₃ occurrence
14 doubles with 4°C of temperature increase in the SMA during high O₃ months (May to
15 October). This implies that those regions will experience frequent high O₃ events in a
16 future warming climate. In terms of short-term variation, the distribution of high O₃
17 probability classified by wind direction shows the effect of both local precursor emissions
18 and long-range transport from China. In terms of long-term variation, the O₃
19 concentrations have increased by +0.26 ppbv yr⁻¹ on nationwide average, but their trends
20 show large spatial variability. Singular value decomposition analyses further reveal that
21 the long-term temporal evolution of O₃ is similar to that of nitrogen dioxide, although the
22 spatial distribution of their trends is different. This study will be helpful as a reference for
23 diagnostics and evaluation of regional- and local-scale O₃ and climate simulations, and as
24 a guide to appropriate O₃ control policy in South Korea.

25

26 **Keywords:** South Korea, surface ozone, KZ-filter, temporal trends, meteorological effects

27

28 **1. Introduction**

29 Surface ozone (O₃) is a well-known secondary air pollutant, which affects air
30 quality, human health, and vegetation. High O₃ concentration has detrimental effects on
31 respiration, lung function, and airway reactivity in human health (Bernard et al., 2001; Bell
32 et al., 2007). In terms of mortality, Levy et al. (2005) have previously assessed that 10
33 ppbv increase in 1-h maximum O₃ could increase daily mortality by 0.41%. High O₃
34 concentrations could also reduce agricultural production. For example, Wang and
35 Mauzerall (2004) reported that the East Asian countries of China, Japan, and South Korea
36 lost 1–9% of their yields of wheat, rice, and corn, and 23–27% of their yields of soybeans
37 due to O₃ in 1990. In addition, O₃ is one of greenhouse gases of which radiative forcing is
38 estimated as the third largest contribution among the various constituents in the
39 troposphere (IPCC, 2007). Therefore, the spatially inhomogeneous distribution of O₃ due
40 to its short chemical lifetime of a week to a month could induce strong regional-scale
41 climate responses (Mickley et al., 2004).

42 In the Northern Hemisphere mid-latitudes where population, industry, and
43 transportation are concentrated, the background O₃ levels increased during the late 20th
44 century due to increases in anthropogenic precursors particularly nitrogen oxides (NO_x),
45 but its trends show regional and temporal differences (Oltmans et al., 1998; Guicherit and
46 Roemer, 2000; Vingarzan, 2004). Although the increasing trends of O₃ in Europe, North
47 Atlantic, North America, and Japan have flattened over the past decade (Oltmans et al.,
48 2006; Oltmans et al., 2013), there have still been concerns about elevated O₃ concentration
49 in China owing to rapid economic growth and industrialization (Ding et al., 2008; Tang et
50 al., 2009; Wang et al., 2009; Wang et al., 2012). Such recent increases of O₃ in China can
51 affect the regional background O₃ levels in East Asia by transboundary transport of O₃ and
52 its precursors. For example, previous modeling studies have shown that the transport of O₃
53 from China by continental outflow is one of the major contributions of O₃ in Japan and
54 South Korea (Tanimoto et al., 2005; Nagashima et al., 2010). Intercontinental transport of
55 O₃ and its precursors originated from East Asia affects O₃ concentrations and air quality in
56 remote areas even on a global scale (Akimoto, 2003). Experiments using a global climate-
57 chemistry model with future emission scenarios by Lei et al. (2013) suggest that the
58 increase in East Asian emissions will still be an important issue for the O₃ air quality in
59 both East Asia and United States.

60 Recently, several studies have focused on the relationship between O₃ levels and
61 temperature, and suggested potential influences of the global warming and climate change

62 on the high levels of O₃ (Jacob and Winner, 2009; Rasmussen et al., 2012; and references
63 therein). Lin et al. (2001) calculated probability of daily maximum 8-h average O₃
64 exceeding 85 ppbv for a given range of daily maximum temperatures and reported that a
65 3°C increase of the daily maximum temperature doubles risk of O₃ exceedances in the
66 Northeastern United States. In addition, Ordóñez et al. (2005) showed that high
67 temperature extremes probably led to the high occurrence of severe O₃ episodes during the
68 summer 2003 heat wave over Europe. These results imply the potentially large sensitivity
69 of O₃ concentration and related air quality to the temperature increases (Jacob and Winner,
70 2009). In the model experiments by Lin et al. (2008), both averaged O₃ concentration and
71 frequencies of high O₃ episodes were predicted to increase in the future over the United
72 States and East Asia. Recent global climate-chemistry model experiments by Lei and
73 Wang (2014) also implied the future O₃ increases in industrial regions due to more O₃
74 production by photochemical reactions and less O₃ removal by nocturnal odd nitrogen
75 (NO_y) chemistry in warmer condition.

76 In South Korea, one of the most highly populated countries in the world, both O₃
77 concentration and high O₃ episodes have increased in recent decades despite efforts to
78 regulate emissions of O₃ precursors (KMOE, 2012). Although the increase of O₃ levels in
79 South Korea over the last three decades is mainly regarded as the results of rapid
80 industrialization, economic expansion, and urbanization, there are other factors to be
81 considered to explain the long-term increase in O₃ concentration. For example, since the
82 Korean peninsula is located on the eastern boundary of East Asia, downward transport of
83 O₃ by the continental outflow considerably affects the high O₃ levels in South Korea (Oh
84 et al., 2010). In addition, recent warming trend related to global climate change could also
85 be an important factor to increase O₃ concentration in South Korea. Climate change is
86 expected to increase both frequency and intensity of temperature extremes over the Korean
87 peninsula (Boo et al., 2006). Therefore, comprehensive understanding of the various
88 factors affecting O₃ concentration, such as local precursor emissions, transport of O₃ and
89 its precursors from local and remote sources, and changes in meteorological fields related
90 to climate change is required to guide environmental policies.

91 The present study aims to examine the spatio-temporal characteristics of the
92 measured O₃ variations in South Korea with consideration of three time scales and various
93 meteorological factors, using ground-measured data from 124 air quality monitoring sites
94 and 72 weather stations for the 12-yr period of 1999–2010. We decomposed O₃ time series
95 at each measurement site into different time scale of short-term, seasonal, and long-term

96 components by application of the Kolmogorov-Zurbenko filter (KZ-filter) that has been
97 used in previous studies (e.g. Gardner and Dorling, 2000; Ibarra-Berastegi et al., 2001;
98 Thompson et al., 2001; Lu and Chang, 2005; Wise and Comrie, 2005; Tsakiri and
99 Zurbenko, 2011; Shin et al., 2012). To investigate the meteorological impact on the O₃
100 levels, we applied the combined analysis of the KZ-filter and linear regression model with
101 the meteorological variables. In the short-term time scale, the possible effects of transport
102 from the local and remote sources on the high O₃ episodes were explored by using the
103 wind data. In the long-term time scale, the singular value decomposition (SVD) with
104 nitrogen dioxide (NO₂) measurements was additionally applied to examine the effects of
105 varying local emissions on the long-term O₃ trend.

106 The remainder of this paper is structured as follows. In the next section, we
107 describe the observational data and analysis techniques used in this study. In Sect. 3, we
108 investigate the spatio-temporal characteristics of the decomposed O₃ time series and its
109 relationship with meteorological variables over South Korea. Finally, the key findings are
110 summarized in Sect. 4.

111

112 **2. Data and methodologies**

113 **2.1. Data**

114 The National Institute of Environmental Research (NIER) of South Korea
115 provides hourly data of O₃ and NO₂ mixing ratios in the ppbv unit, which have been
116 measured by ultraviolet absorption and chemiluminescence respectively. We here select
117 124 urban air quality monitoring sites over South Korea, based on data availability for the
118 period 1999–2010, and analyze hourly time series of O₃ and NO₂ from each site. It is noted
119 that our current analysis exclude other data from roadside measurement sites where data
120 can be directly affected by the vehicle exhaust emissions and suburban and background
121 sites located around South Korea. Hourly meteorological data at 72 weather stations of the
122 Korea Meteorological Administration (KMA) for the same period are also used to examine
123 the effects of meteorological factors on the O₃ variations. The meteorological variables
124 used in this study include common factors related to the O₃ variations such as temperature
125 (°C), surface insolation (W m⁻²), relative humidity (%), and wind speed (m s⁻¹) (e.g.
126 Ordóñez et al., 2005; Camalier et al., 2007; Jacob and Winner, 2009). Dew-point
127 temperature (°C) and sea-level pressure (hPa) are additionally applied for multiple linear
128 regression models as other previous studies have done (e.g., Thompson et al., 2001; Shin
129 et al., 2012). Finally wind direction (16 cardinal directions) is used to reveal its

130 relationship with short-term changes in O₃. Using the hourly data, we first calculated daily
131 averages for O₃ (O_{3 avg}), NO₂ (NO_{2 avg}), temperature (*T*), surface insolation (SI), dew-point
132 temperature (TD), sea-level pressure (PS), wind speed (WS), wind direction (WD), and
133 relative humidity (RH). We also obtained daily minimum O₃ (O_{3 min}), daily maximum 8-h
134 average O₃ (O_{3 8h}), and daily maximum temperature (*T*_{max}) from the hourly data set.

135 To investigate the relationship between O₃ and meteorological variables, it is
136 desirable to use data observed at the same stations. However, not all of air quality
137 monitoring sites and weather stations are closely located in South Korea. Therefore, we
138 assume that an air quality monitoring site can observe the same meteorological variables
139 as those at a weather station if the distance between the two places is less than 10 km.
140 Under the assumption, only O₃ data from 72 air quality monitoring sites and
141 meteorological data from 25 weather stations are available to analyze the meteorological
142 effects on the O₃ variation over South Korea. The insolation was measured only at 17
143 weather stations for the analysis period. Figure 1 shows geographical locations of the
144 ground measurements used in the present study, together with colored topography based
145 on the U.S. Geological Survey (USGS) Digital Elevation Model (DEM).

146

147 **2.2. Decomposition of O₃ time series by KZ-filter**

148 The KZ-filter is a decomposition method than can be used to separate time series
149 into short-term, seasonal, and long-term components (Rao and Zurbenko, 1994). We
150 applied the KZ-filter to the O₃ time series by taking moving average of window length *m*
151 with iterating *p* times, which is denoted by KZ_{*m,p*}. The KZ-filter is basically low-pass filter
152 for removing high frequency components from the original time series. Following
153 Eskridge et al. (1997), the KZ-filter removes the signal smaller than the period *N*, which is
154 called as the effective filter width. *N* is defined as follows:

$$155 \quad m \times p^{1/2} \leq N \quad (1)$$

156 The KZ-filter method has the same level of accuracy as the wavelet transform
157 method although it is much easier way to decompose the original time series (Eskridge et
158 al., 1997). In addition, time series with missing observations can be applicable to KZ-filter
159 owing to the iterative moving average process.

160 For the clear separation of the components, we applied KZ-filter to the daily log-
161 transformed O₃ as in Rao and Zurbenko (1994) and Eskridge et al. (1997), instead of the
162 raw O₃ concentrations. While the short-term component separated by the KZ-filter using

163 raw O₃ data still shows clear seasonality, use of $\ln(O_3)$ makes the short-term component
 164 stationary and nearly independent of the seasonal influence by stabilizing variance (Rao
 165 and Zurbenko, 1994; Rao et al., 1997). Note that a temporal linear trend of log-
 166 transformed data is provided as % yr⁻¹ because the differential of the natural logarithm is
 167 equivalent to the percentage change.

168 The natural logarithm of the O₃ time series at each site denoted as $[O_3](t)$ is thus
 169 decomposed by KZ-filter as follows:

$$170 [O_3](t) = [O_{3\text{ST}}](t) + [O_{3\text{SEASON}}](t) + [O_{3\text{LT}}](t) \quad (2)$$

171 $[O_{3\text{ST}}]$ is a short-term component attributable to day-to-day variation of synoptic-
 172 scale weather and short-term fluctuation in precursor emissions. $[O_{3\text{SEASON}}]$ represents a
 173 seasonal component related to the seasonal changes in solar radiation and vertical transport
 174 of O₃ from the stratosphere whose time scale is from several weeks to months. $[O_{3\text{LT}}]$
 175 denotes a long-term component explained by changes in precursor emission, transport,
 176 climate, policy, and economy over the entire period (Rao et al., 1997; Milanchus et al.,
 177 1998; Gardner and Dorling, 2000; Thompson et al., 2001; Wise and Comrie, 2005).
 178 Tsakiri and Zurbenko (2011) showed that $[O_{3\text{ST}}]$ and $[O_{3\text{LT}}]$ are independent of each other.
 179 Also, statistical characteristics of $[O_{3\text{ST}}]$ are very close to those of white noise (Flaum et
 180 al., 1996) and therefore, $[O_{3\text{ST}}]$ is nearly detrended.

181 In this study, we used the KZ-filter with the window length of 29 days and 3
 182 iterations (KZ_{29,3}) following previous studies (e.g., Rao and Zurbenko, 1994) and
 183 decomposed daily $\ln(O_{3\text{8h}})$ time series at the 124 monitoring sites. KZ_{29,3} removes $[O_{3\text{ST}}]$
 184 with period shorter than about 50 days, following Eq. (1). We defined the filtered time
 185 series as a baseline ($[O_{3\text{BL}}]$) as in Eq. (3).

$$186 [O_3](t) = [O_{3\text{BL}}](t) + [O_{3\text{ST}}](t) \quad (3)$$

187 Eq. (3) accounts for the multiplicative effects of short-term fluctuations on the $[O_3]$
 188 $[O_{3\text{BL}}]$ due to the log-transformation (Thompson et al., 2001). In other words, exponential of
 189 $[O_{3\text{ST}}]$ is a ratio of the raw O₃ concentrations to the exponential of $[O_{3\text{BL}}]$, which is the
 190 baseline O₃ concentration in ppbv. Therefore, if $\exp[O_{3\text{ST}}]$ is larger than 1, the raw O₃
 191 concentration will be larger than the baseline O₃ concentration.

192 $[O_{3\text{BL}}]$ is expressed as the sum of $[O_{3\text{SEASON}}]$ and $[O_{3\text{LT}}]$, as in Eq. (4) (Milanchus
 193 et al., 1998).

$$194 [O_{3\text{BL}}](t) = [O_{3\text{SEASON}}](t) + [O_{3\text{LT}}](t) \quad (4)$$

195 Since $[O_3]_{BL}$ is closely associated with meteorological fields, we built a multiple
 196 regression model with available meteorological variables as in Eq. (5), following previous
 197 studies (e.g., Rao and Zurbenko, 1994; Rao et al., 1995; Ibarra-Berastegi et al., 2001).
 198 Short-term variability of meteorological variables was also filtered out by $KZ_{29,3}$.

$$199 \quad [O_3]_{BL}(t) = a_0 + \sum_i a_i MET_{BL}(t)_i + \varepsilon(t) \quad (5)$$

$$MET_{BL}(t) = [T_{max\ BL}(t), SI_{BL}(t), TD_{BL}(t), PS_{BL}(t), WS_{BL}(t), RH_{BL}(t)]$$

200 In the multiple linear regression model, $[O_3]_{BL}$ is a response variable and the
 201 baselines of meteorological variables ($MET_{BL}(t)_i$) are predictors. Also, a_0 , a_i , and $\varepsilon(t)$
 202 denote the constant, regression coefficient of variable i , and residual of the multiple
 203 regression model, respectively.

204 The residual term $\varepsilon(t)$ contains not only the long-term variability of O_3 related to
 205 long-term changes in local precursor emissions but also seasonal variability of O_3
 206 attributable to unconsidered meteorological factors in the multiple linear regression model.
 207 Thus, we applied the KZ-filter with the window length of 365 days and 3 iterations
 208 ($KZ_{365,3}$) to $\varepsilon(t)$ to extract the meteorologically adjusted $[O_3]_{LT}$ of which the period is
 209 larger than about 1.7 yr as follow:

$$210 \quad \varepsilon(t) = KZ_{365,3}[\varepsilon(t)] + \delta(t) = [O_3]_{LT}(t) + \delta(t) \quad (6)$$

211 In Eq. (6), $\delta(t)$ denotes the seasonal variability of O_3 related to the meteorological
 212 variables unconsidered in the multiple linear regression model and/or noise.

213 Finally, $[O_3]_{SEASON}$ is obtained by sum of the combined meteorological variables
 214 regressed on $[O_3]_{BL}$ ($a_0 + \sum_i a_i MET_{BL}(t)_i$) and $\delta(t)$ as in Eq. (7).

$$215 \quad [O_3]_{SEASON}(t) = a_0 + \sum_i a_i MET_{BL}(t)_i + \delta(t) \quad (7)$$

216 Figure 2 shows a schematic representation of Eq. (2) using daily O_3 $8h$ time series
 217 at the City Hall of Seoul for the period of 1999–2010. $[O_3]_{SEASON}$ in Fig. 2c clearly shows
 218 the typical seasonal cycle of O_3 in South Korea with high concentrations in spring, slight
 219 decrease in July and August, and increase in autumn (Ghim and Chang, 2000). The spring
 220 maximum of O_3 concentration in the Northern Hemisphere is generally attributed to
 221 episodic stratospheric intrusion (Levy et al., 1985; Logan, 1985), photochemical reactions
 222 of accumulated NO_x and hydrocarbons during the winter (Dibb et al., 2003), accumulation
 223 of O_3 due to the longer photochemical lifetime (~ 200 days) during the winter (Liu et al.,
 224 1987), and transport of O_3 and its precursors by the continental outflow (Carmichael et al.,
 225 1998; Jacob et al., 1999; Jaffe et al., 2003). On the other hand, frequent precipitation

226 during the East Asian summer monsoon influences the decrease of O₃ concentrations in
227 July and August (Ghim and Chang, 2000). [O₃ LT] in Fig. 2d shows that the O₃
228 concentrations at the monitoring site have increased in the past decade, irrespective of any
229 change in meteorological conditions. It should be noted that [O₃ LT] explains only 1.7% of
230 the total variance of [O₃] at this site as can be seen from its small ranges in Fig. 2d, while
231 relative contributions of [O₃ ST] and [O₃ SEASON] are 58.3% and 32.7%, respectively.
232 Therefore, the long-term changes in O₃ related to changes in local emission are only a
233 small fraction of the O₃ variations. The relative contributions of each component are
234 further examined in Sect. 3.4.

235

236 **2.3. Spatial interpolation by AIDW method**

237 The inverse-distance weighting (IDW) is a deterministic spatial interpolation
238 technique for spatial mapping of variables distributed at irregular points. In this study, we
239 adopted the enhanced version of the IDW, the adaptive inverse-distance weighting
240 (AIDW) technique (Lu and Wong, 2008). While the traditional IDW uses a fixed distance-
241 decay parameter without considering the distribution of data within it, the AIDW uses
242 adjusted distance-decay parameters according to density of local sampling points.
243 Therefore, the AIDW provides flexibility to accommodate variability in the distance-decay
244 relationship over the domain and thus better spatial mapping of variables distributed at
245 irregular observational points (Lu and Wong, 2008).

246 In the mapping of O₃ with spatial interpolation, there are ubiquitous problems
247 such as spatial-scale violations, improper evaluations, inaccuracy, and inappropriate use of
248 O₃ maps in certain analyses (Diem, 2003). The spatial mapping in the present study also
249 has problems with the spatial resolution of the observations, which is not high enough to
250 consider small-scale chemical processes and geographical complexity of the Korean
251 peninsula (see Fig. 1). Most of the air quality monitoring sites are concentrated on the
252 cities, and typical inter-city distances are 30–100 km in South Korea while spatial
253 representativeness of O₃ concentration is possibly as small as around 3–4 km (Tilmes and
254 Zimmermann, 1998) or 5 km (Diem, 2003). In addition, mapping with a few monitoring
255 sites combined with complex mountainous terrain can also distort the actual distribution of
256 data, especially in the northeastern part of South Korea. Despite such limits, the spatial
257 mapping in this study is still useful because we aim not to derive an exact value at a
258 specific point where the observation does not exist, but to provide the better quantitative

259 understanding of O₃ and related factors in South Korea, especially focused on the
260 metropolitan and urban areas.

261

262 **3. Results**

263 **3.1. Spatial characteristics of O₃ and its trend in South Korea**

264 Climatological daily average O₃ (O_{3 avg}) and its temporal linear trends are
265 represented in Fig. 3 and Table 1 using data from 124 monitoring sites distributed
266 nationwide in 46 cities for the past 12-yr period. The spatial map of climatological daily
267 average NO₂ (NO_{2 avg}) is also shown in Fig. 3. In Table 1, the cities are categorized into
268 three geographical groups: 16 coastal cities, 14 inland cities, and 16 cities in the Seoul
269 Metropolitan Area (SMA). We separated the SMA cities from the other two groups since
270 the SMA is the largest source region of anthropogenic O₃ precursors in South Korea. The
271 SMA occupies only 11.8% (11,745 km²) of the national area, but has 49% (25.4 million)
272 of the total population and 45% (8.1 million) of total vehicles in South Korea. It is
273 estimated that approximately 27% (0.29 Mt) of total NO_x emissions and 34% (0.30 Mt) of
274 the volatile organic compounds (VOCs) emissions in South Korea are from the SMA in
275 2010 (KMOE, 2013). Therefore, the climatological NO_{2 avg} concentration in the SMA is
276 much higher than that in other region (Fig. 3b).

277 In general, O₃ concentrations are high at the coastal cities, low at the inland cities,
278 and lowest at the SMA cities in South Korea. Along with Table 1, Fig. 3a shows that the
279 12-yr average of O_{3 avg} is high at the southern coastal cities such as Jinhae (31.3 ppbv),
280 Mokpo (30.3 ppbv), and Yeosu (28.1 ppbv), with the highest value at Jeju (32.6 ppbv), and
281 low at the inland metropolitan cities such as Daegu (19.8 ppbv), Gwangju (20.5 ppbv), and
282 Daejeon (20.7 ppbv), with lowest values at the SMA cities including Seoul (17.1 ppbv),
283 Incheon (19.0 ppbv) and Anyang (16.8 ppbv).

284 Compared to the regional background concentration of 35–45 ppbv at five
285 background measurement sites around South Korea (KMOE, 2012), the averaged O₃
286 concentrations in the SMA and inland metropolitan cities are much lower while those at
287 the coastal cities are close to the regional background levels. In comparison with Fig. 3b,
288 Fig. 3a shows that relatively lower O_{3 avg} regions are well consistent with relatively higher
289 NO_{2 avg} regions. Substantial emissions of anthropogenic NO in the SMA and other inland
290 metropolitan cities lead to NO_x titration effects even in the absence of photochemical
291 reactions during the night, and thus the averaged O₃ concentrations are depressed by 10–20
292 ppbv lower than the regional background concentration (Ghim and Chang, 2000). A recent

293 modeling study by Jin et al. (2012) has suggested that the maximum O₃ concentrations in
294 the SMA, especially in Seoul and Incheon, are VOCs-limited. In the coastal region, on the
295 other hand, low emissions of NO with dilution by the strong winds weaken the titration
296 effect and result in the high O₃ concentrations. The dynamic effect of land-sea breeze is
297 another possible factor of the high O₃ levels at the coastal cities. Oh et al. (2006) showed
298 that a near-stagnant wind condition at the development of sea breeze temporarily contains
299 O₃ precursors carried by the offshore land breeze during the night, and following
300 photochemical reactions at mid-day produces O₃. The relationship between O₃ and wind
301 speed and direction will be shown in Sects. 3.2 and 3.5 respectively.

302 In terms of temporal trends, the surface O₃ concentrations in South Korea have
303 generally increased for the past 12 yr as shown in Fig. 3c and Table 1. The averaged
304 temporal linear trend of O₃ _{avg} at 46 cities nationwide is +1.15% yr⁻¹ (+0.26 ppbv yr⁻¹),
305 which is comparable with observed increasing trends of approximately +0.5–2% yr⁻¹ in
306 various regions in the Northern Hemisphere (Vingarzan, 2004). Compared with previous
307 studies in East Asia, the overall increasing trend of O₃ in South Korea is smaller than
308 recent increasing trends over China of +1.1 ppbv yr⁻¹ in Beijing for 2001–2006 (Tang et al.,
309 2009) and +0.58 ppbv yr⁻¹ in Hong Kong for 1994–2007 (Wang et al., 2009) but slightly
310 larger than increasing trend over Japanese populated areas of +0.18 ppbv yr⁻¹ for 1996–
311 2005 (Chatani and Sudo, 2011).

312 Several factors that could influence the overall increase of O₃ over East Asia were
313 suggested by the following previous studies. Recently, Zhao et al. (2013) have estimated
314 that the NO_x emissions in China increased rapidly from 11.0 Mt in 1995 to 26.1 Mt in
315 2010, mainly due to the fast growth of energy consumption. The NO_x and VOCs emissions
316 in South Korea also increased in the early 2000s. The estimated anthropogenic NO_x and
317 VOCs emissions are 1.10 Mt and 0.74 Mt in 1999 but 1.35 Mt and 0.87 Mt in 2006,
318 respectively (KMOE, 2013). Tanimoto et al. (2009) suggested that the O₃ increase results
319 from such recently increased anthropogenic precursor emissions in East Asia.

320 However, model sensitivity simulations in Chatani and Sudo (2011) indicate that
321 the changes in East Asian emissions can explain only 30% of the O₃ trend. They have
322 suggested the long-term variations in meteorological fields as a possible important factor
323 although further studies are required. In particular, it is well known that insolation and
324 temperature are important meteorological factors in O₃ variation. While insolation directly
325 affects O₃ production through photochemical reactions, increased temperature affects net
326 O₃ production rather indirectly by increasing biogenic hydrocarbon emissions, hydroxyl

327 radical (OH) with more evaporation, and NO_x and HO_x radicals by thermal decomposition
328 of peroxyacetyl nitrate (PAN) reservoir (Sillman and Samson, 1995; Olszyna et al., 1997;
329 Racherla and Adams, 2006; Dawson et al., 2007). Therefore, the O₃ increasing trend in Fig.
330 3c is possibly affected by changes in meteorological variables.

331 Figure 4 shows temporal linear trends of daily average temperature (*T*) and
332 insolation (SI). Despite the spatial discrepancy between trends of O₃ (Fig. 3c) and
333 meteorological variables (Fig. 4), both temperature and insolation have generally increased
334 in South Korea for the past 12 yr. The spatial mean of temporal linear trend in temperature
335 at 72 weather stations nationwide is approximately +0.09°C yr⁻¹, which is much higher
336 than +0.03°C yr⁻¹ for the Northern Hemispheric land surface air temperature for 1979–
337 2005 (IPCC, 2007). This high increasing trend of temperature in South Korea is probably
338 due to urban heat island effect with rapid urbanization. The averaged temporal linear trend
339 of insolation at 22 weather stations nationwide is about +1.47 W m⁻² yr⁻¹ despite the
340 decreasing phase of solar cycle during the 2000s. This is possibly caused by reduction in
341 particulate matter emissions due to enhanced environment regulation in South Korea
342 during the recent decade (KMOE, 2012).

343 Although O₃ and related meteorological variables such as temperature and
344 insolation have recently increased in South Korea, the spatial patterns of their temporal
345 trends do not show clear similarity. In addition, the spatial distribution of O₃ trends is
346 rather inhomogeneous even on a metropolitan scale. For instance, Table 1 shows a wide
347 range of O₃ trends among the SMA cities from -1.25% yr⁻¹ of Gwacheon to +2.82% yr⁻¹ of
348 Seoul. The spatial inhomogeneity in O₃ trend and the trend differences among O₃,
349 temperature, and insolation imply that the long-term O₃ trends in South Korea are not only
350 affected by changes in meteorological conditions but also influenced by changes in local
351 precursor emissions or transport of O₃ and its precursors. The local effects of precursor
352 emissions on the long-term changes in O₃ are further examined in Sect 3.6.

353

354 **3.2. Relationships between O₃ and meteorological variables**

355 A multiple linear regression model is here adopted to explain relationships
356 between O_{3 8h} and each of key meteorological variables such as *T*_{max}, SI, TD, PS, WS, and
357 RH. To exclude day-to-day short-term fluctuations or white noises from the original time
358 series, KZ_{29,3} was applied to each variable before the regression process and yielded
359 baselines of each variable. As a result of the multiple linear regression, coefficients of
360 determination (*R*²) between baselines of O_{3 8h} and each meteorological variable, as well as

361 adjusted R^2 for the multiple linear regression models, were calculated for 72 air quality
362 monitoring sites distributed in 25 cities nationwide and summarized in Table 2. Combined
363 meteorological effects on O_3 variations in each city are represented by adjusted R^2 , which
364 adjusts for the number of predictors with consideration of the degrees of freedom. The
365 nationwide average of adjusted R^2 is 0.51 and that of R^2 is 0.50 for SI, 0.29 for PS, 0.22 for
366 T_{\max} , 0.14 for TD, 0.05 for RH, and 0.03 for WS, respectively. In South Korea, SI, T_{\max} ,
367 and TD generally show positive correlations with O_3 levels while PS is negatively
368 correlated with O_3 variations. Since the short-term variability in each variable is excluded,
369 the negative correlation between O_3 and PS is related to their seasonal cycle rather than
370 continuously changing weather system of high and low. PS in South Korea located on the
371 continental east coast is mostly affected by the cold continental high pressure air mass
372 during the winter when the O_3 concentrations are lowest. On the other hand, WS and RH
373 show weak correlations with O_3 variations.

374 The spatial distributions of R^2 for T_{\max} and SI, as well as the adjusted R^2 for the
375 combined meteorological effects, are represented in Fig. 5. Both Figs. 5a and 5b show a
376 common spatial pattern with high correlations at the inland and SMA cities and low
377 correlations at the coastal cities. For instance, the average R^2 value with T_{\max} for the
378 coastal cities is only 0.07, which is much smaller than 0.36 for the SMA cities and 0.30 for
379 the inland cities. Also, the average R^2 values with SI are 0.60 for the SMA cities and 0.58
380 for the inland cities, but 0.35 for the coastal cities. Despite the similar pattern between Figs.
381 5a and 5b, the R^2 values of SI are much higher than those of T_{\max} because temperature
382 affects net O_3 production rather indirectly compared to the direct influence of insolation on
383 O_3 levels by photochemical production (Dawson et al., 2007; and references therein). The
384 apparent R^2 differences among three regions indicate that temporal variations of O_3 at the
385 SMA and inland cities are much more sensitive to SI and T_{\max} than those at the coastal
386 cities. The low dependence of O_3 on T_{\max} and SI at the coastal cities means that the
387 photochemical reactions of precursors are less important for determining O_3 levels there
388 compared to the SMA and inland cities.

389 The meteorological effects on O_3 at the inland, coastal, and SMA cities are also
390 examined by daily minimum O_3 ($O_{3\min}$). As represented in Fig. 6a and Table 3, the $O_{3\min}$
391 is high near the coast, low at the inland cities, and lowest in the SMA. In the polluted
392 urban area, the O_3 concentration reaches near-zero minima during the night since O_3 is
393 reduced by NO_x titration, nocturnal NO_y chemical process related to nitrate formation, and
394 dry deposition in the absence of photochemical production. However, in the coastal region

395 where the NO_x concentrations are low (Fig. 3b), the lower titration and nitrate formation at
396 nighttime lead to the higher O_3 $_{\text{min}}$ levels. In addition, transport of O_3 from the regional
397 background could also keep high levels of O_3 during the night (Ghim and Chang, 2000).
398 Frequency distributions of O_3 concentrations in previous studies suggested that O_3 levels at
399 the coastal cities such as Gangneung, Jeju, Mokpo, Seosan, and Yeosu are affected by the
400 background O_3 transport, unlike Seoul where the effect of local precursor emission is
401 dominant (Ghim and Chang, 2000; Ghim, 2000). Therefore, combined effects of the low
402 NO_x levels and transport of the regional background O_3 influence the high O_3 $_{\text{min}}$ near the
403 coast.

404 Compared to the spatial distribution of R^2 between baselines of O_3 $_{8\text{h}}$ and T_{max} or
405 SI (Figs. 5a and 5b), O_3 $_{\text{min}}$ distribution in Fig. 6a shows high O_3 $_{\text{min}}$ at the coastal cities
406 where the R^2 is low and low O_3 $_{\text{min}}$ at the inland cities where the R^2 is high. These opposite
407 patterns suggest that the meteorological effects on the O_3 production are negatively
408 correlated with O_3 $_{\text{min}}$ for the South Korean cities. The clear negative correlations are also
409 shown in scatter plots (Figs. 6b and 6c). In both scatter plots, the three geographical groups
410 of cities (blue for the coastal cities, green for the inland cities and red for SMA) are well
411 separated. Several industrial or metropolitan cities in the coastal region such as Changwon
412 (CW), Busan (BS), and Ulsan (US) have relatively low O_3 $_{\text{min}}$ compared to the rest of
413 coastal cities. Larger NO_x emissions in these southeastern coastal cities (Fig. 3b) induce
414 lower O_3 $_{\text{min}}$ levels via NO_x titration and nocturnal NO_y chemical process. Among the SMA
415 cities, on the other hand, Ganghwa (GH) has much higher O_3 $_{\text{min}}$ compared to other SMA
416 cities. Ganghwa is a rural county located on the northwestern coast of the SMA. Therefore,
417 both small NO_x emissions there and transport of regional background O_3 from the Yellow
418 Sea affect the characteristics of O_3 in Ganghwa.

419 The different meteorological effects on O_3 between the coastal and inland regions
420 are further examined with wind speed. Daily average wind speed (WS) data over South
421 Korea are averaged for 12 yr. The 12-yr averaged WS are summarized in Table 3 and
422 presented in spatial map of Fig. 7a, which show high wind speed in the coastal region and
423 low wind speed in the inland region. Figures 7b and c show that the averaged wind speeds
424 at 25 cities are positively correlated with O_3 $_{\text{min}}$ and negatively correlated with the R^2
425 between O_3 and T_{max} . In general, surface mixing and ventilation by high wind speeds
426 reduce the precursors near surface and thus decrease the photochemical production of O_3 .
427 Therefore the relationship between high wind speed and high O_3 levels in the coastal
428 region is attributable to the transport of background O_3 . On the other hand, the weaker

429 wind speed induces more effective photochemical reaction through the longer reaction
430 time in stagnant condition as well as more enhanced aerodynamic resistance to dry
431 deposition (Jacob and Winner, 2009). Therefore, the effects of insolation and temperature
432 on the O₃ productions become more important in the inland region where the wind speeds
433 are lower.

434

435 **3.3. Probability of O₃ exceedances related to temperature**

436 Evaluating the probability of O₃ exceeding the air quality standard in a given
437 range of temperature is useful to speculate about potential sensitivity of O₃ concentration
438 to climate change (Lin et al., 2001; Jacob and Winner, 2009). Here we calculate the
439 probabilities that O_{3 8h} exceeds the Korean air quality standard of 60 ppbv (KMOE, 2012)
440 as a function of the daily maximum temperature (T_{\max}) for the coastal, inland, and SMA
441 cities. Similar to the analyses in Lin et al. (2001) for the contiguous United States, Fig. 8
442 shows that the probabilities of O₃ exceedances increase with T_{\max} at the inland and SMA
443 cities. For example, the probability of O₃ exceedances in the SMA is almost doubled by
444 about 4°C increase in T_{\max} and reach 27% at 30°C. In the coastal region, on the other hand,
445 the probability of O₃ exceedance increases up to 12–13% with T_{\max} change from 10°C to
446 20°C and does not increase significantly for T_{\max} above 20°C. This is consistent with the
447 spatial feature of the meteorological effects on O₃ levels, which are high at the inland and
448 SMA cities and low at the coastal cities as described in the previous section. Therefore, the
449 probability of high O₃ occurrence will be more sensitive to the future climate change at the
450 inland and SMA cities than at the coastal cities. In the previous modeling study by Boo et
451 al. (2006), T_{\max} over the Korean peninsula is expected to rise by about 4–5°C to the end of
452 21st century owing to global warming. This suggests considerable future increases in
453 exceedances of the O₃ air quality standard over South Korea, except over coastal regions,
454 in the absence of emission abatement measures.

455

456 **3.4. Relative contributions of O₃ variations in different time scales**

457 Surface O₃ variation can be decomposed into short-term component ($[O_3_{ST}]$),
458 seasonal component ($[O_3_{SEASON}]$), and long-term component ($[O_3_{LT}]$) by using the KZ-
459 filter as described in Sect. 2.2. We evaluated relative contributions of each component to
460 total variance of original time series. Overall, the relative contributions of $[O_3_{LT}]$ in Fig.
461 9c are much smaller than those of $[O_3_{ST}]$ in Fig. 9a and $[O_3_{SEASON}]$ in Fig. 9b at all cities
462 (Table 4). Therefore, sum of $[O_3_{ST}]$ and $[O_3_{SEASON}]$ account for the most of O₃ variations.

463 In Figs. 9a and 9b, the relative contributions of $[O_3_{ST}]$ and $[O_3_{SEASON}]$ show a
464 strong negative relationship spatially. The relative contributions of $[O_3_{ST}]$ are generally
465 larger at the coastal cities (53.1%) than at the inland cities (45.9%), whereas the relative
466 contributions of $[O_3_{SEASON}]$ are smaller at the coastal cities (32.8%) than at the inland
467 cities (41.9%).

468 Since $[O_3_{ST}]$ is related to synoptic-scale weather fluctuation (Rao et al., 1995; Rao
469 et al., 1997), the large relative contributions of $[O_3_{ST}]$ at the coastal cities indicate the
470 stronger effects of the eastward moving synoptic weather systems there. Interestingly, the
471 highest value of $[O_3_{ST}]$ contribution appears at a northeastern coastal city, Gangneung.
472 High and steep mountains on the west of Gangneung induce often warm, dry, and strong
473 westerly winds, which is favorable to the clear sky and strong vertical mixing over the
474 region. Since the westerly winds contain the precursors emitted from the SMA, the clear
475 sky condition increases the O_3 levels during the daytime. In addition, the strong vertical
476 mixing of high O_3 air from the free troposphere compensates the O_3 loss by titration during
477 the nighttime. In the easterly winds, however, orographic lift often forms fog or clouds
478 over the region and reduces the photochemical production of O_3 . Therefore, combined
479 effects of wind directions related to synoptic weather systems and topography increase the
480 short-term variability of O_3 at Gangneung.

481 On the other hand, $[O_3_{SEASON}]$ is driven mainly by the annual cycle of
482 meteorological factors such as insolation or temperature. Therefore, the large relative
483 contributions of $[O_3_{SEASON}]$ at the inland cities are consistent with the higher impacts of
484 temperature and insolation on O_3 there (Figs. 5 and 9b). The highest and second highest
485 values of $[O_3_{SEASON}]$ contribution appear at Andong and Wonju located in the inland basin.
486 Since the basin topography often traps pollutants and induces large annual ranges of
487 temperature, seasonal variability of O_3 at the two cities is larger than that of other inland
488 cities.

489 $[O_3_{LT}]$ explain less than 10% of the total variances, but its relative contribution is
490 considerable in the southwestern part of the Korean peninsula as displayed in Fig. 9c. This
491 is related to relatively large long-term variability or trend in the region and is further
492 discussed in Sect. 3.6.

493

494 **3.5. Short-term variation of O_3 related to wind direction**

495 The short-term components of O_3 ($[O_3_{ST}]$) account for a large fraction of total O_3
496 variation over South Korea. In Table 4, relative contributions of $[O_3_{ST}]$ range from 32.7%

497 to 62.5% and have a nationwide average of 49.8%. Therefore, it is no wonder that high O₃
498 episodes are mostly determined by day-to-day fluctuation of [O_{3 ST}]. One considerable
499 factor influencing the short-term variation of O₃ is wind. Shin et al. (2012) displayed [O₃
500 ST] on the wind speed-direction domain and showed that the effects of episodic long-range
501 transport and local precursor emission on the ambient O₃ concentrations could be
502 qualitatively separated from [O_{3 ST}].

503 We here further investigate the transport effect on the short-term variations of O₃
504 and the frequency of high O₃ episodes using exp[O_{3 ST}] and wind directions (WDs). As
505 described in Sect. 2.2, exp[O_{3 ST}] is a ratio of the raw O_{3 8h} concentration to its baseline
506 concentration in ppbv (exp[O_{3 BL}]). Thus, the O_{3 8h} concentration is higher than the
507 baseline O_{3 8h} concentration when exp[O_{3 ST}] > 1. We classified every single value of
508 exp[O_{3 ST}] by 8 cardinal WDs during the months of frequent high O₃ events (May–
509 October) at all available monitoring sites within each city. The probabilities of exp[O_{3 ST}]
510 > 1 by each WD were compared with the probabilities exceeding the South Korean air
511 quality standard of 60 ppbv for O_{3 8h}.

512 Figure 10 shows exp[O_{3 ST}] in the SMA cities (Seoul, Incheon, Suwon, and
513 Ganghwa) with probabilities of exp[O_{3 ST}] > 1 and O_{3 8h} > 60 ppbv for each WD. In Seoul,
514 high O₃ episodes occur most in northwesterly although westerly and northeasterly winds
515 predominate during the months of frequent high O₃ events (Figs. 10a and 10b). The high
516 probability of high O₃ in northwesterly in Seoul is similar to those in other neighboring
517 cities in SMA, where the predominant probability also appears in northwesterly wind in
518 Incheon located in the west of Seoul (Figs. 10c and 10d), westerly wind in Suwon in the
519 south of Seoul (Figs. 10e and 10f), and Ganghwa in the northwest of Seoul (Figs. 10g and
520 10h).

521 Sea-mountain breeze can explain the prevalence of high O₃ episodes under
522 westerly or northwesterly winds in the SMA. In the western coast of the SMA, there are
523 many thermoelectric power plants (see triangles in Figs. 11 and 12) and industrial
524 complexes, which directly emit a large amount of O₃ precursors. Heavy inland and
525 maritime transportation in those regions is also an important source of NO_x and
526 hydrocarbon emissions. Since the SMA is surrounded by the Yellow Sea in the west and
527 mountainous region in the east (see Fig. 1), the westerly sea breeze is well developed
528 under O₃-conducive meteorological conditions such as high temperature and strong
529 insolation with low wind speed (Ghim and Chang, 2000; Ghim et al., 2001). In addition,
530 locally emitted precursors and transported background O₃ from the west are trapped in the

531 SMA due to the westerly sea breeze and the mountainous terrain in the east of the SMA.
532 Therefore, the O_3 concentrations in the SMA increase in such O_3 -conductive
533 meteorological conditions with near-westerly winds.

534 Another factor to increase the high O_3 probabilities in the near-westerly winds is
535 long-range transport of O_3 and its precursors from China. For example, Ghim et al. (2001)
536 reported some high O_3 cases in the SMA, which result from the transport of O_3 -rich air
537 with strong westerly wind at dawn under overcast conditions. Oh et al. (2010) also showed
538 that the elevated layer of high O_3 concentration over the SMA is associated with the long-
539 range transport of O_3 from eastern China. As the mixing layer thickens over the SMA, the
540 O_3 concentration can increase by up to 25% via vertical down-mixing process (Oh et al.,
541 2010). Recently, Kim et al. (2012) showed that westerly winds also transport O_3 precursors
542 such as NO_2 and carbon monoxide (CO) from China to South Korea.

543 Interestingly, the high O_3 probability in Ganghwa (Figs. 10g and 10h) shows
544 bimodal distribution with another peak in easterly wind. Considering that Ganghwa is a
545 rural county on the northwestern coast of the SMA, the double peak of high O_3 probability
546 in easterly and westerly winds shows the effects of both local and long-range transport.

547 We extended the above $\exp[O_{3\ ST}]$ and WDs analysis to 25 cities over South Korea.
548 The nationwide view of the high O_3 probabilities is represented by the probabilities of
549 $\exp[O_{3\ ST}] > 1$ and $O_{3\ 8h} > 60$ ppbv by each wind direction during the months of frequent
550 high O_3 events (May–October). Figures 11 and 12 show spatial maps of the probabilities
551 of $\exp[O_{3\ ST}] > 1$ and $O_{3\ 8h} > 60$ ppbv, respectively. As indicators of major precursor
552 emission point source, we marked 26 of major thermoelectric power plants with triangles
553 on the map. In general, the most of the thermoelectric power plants are located in the
554 western coast of the SMA and southeastern coastal region of the Korean peninsula.
555 Thermoelectric power plants are important sources of NO_x in South Korea, accounting for
556 13% (0.14 Mt) of total NO_x emission nationwide (KMOE, 2013). Considering that
557 industrial complexes over South Korea are mostly concentrated near the power plants, the
558 area with triangles in Figs. 11 and 12 represents major sources of O_3 precursors.

559 In Figs. 11 and 12, the both probabilities of $\exp[O_{3\ ST}] > 1$ and $O_{3\ 8h} > 60$ ppbv are
560 generally high on a national scale in the near-westerly wind conditions (Figs. 11f–h and 12
561 f–h). The prevailing westerly wind of the synoptic-scale flow transports O_3 and its
562 precursors from China to South Korea and thus increases the probability of high O_3
563 episodes as well as high O_3 concentrations. However, on a local scale, the high probability
564 regions of high O_3 correspond to downwind of the thermoelectric power plants. For

565 example, the high probabilities of high O₃ in the southeastern part of South Korea,
566 downwind of power plants along the southeastern coast, also appear even in the easterly or
567 southerly wind (Figs. 11c–e and 12c–e). Therefore, the spatial features of the high O₃
568 probabilities in each wind direction could be associated with both local effect of precursor
569 emission and long-range transport from the continent.

570

571 **3.6. Long-term variation of O₃ and local precursor emissions**

572 The temporal linear trend of baseline ([O₃ BL]) is almost the same as that of the
573 original time series since short-term component ([O₃ ST]) is nearly detrended. Therefore,
574 the O₃ trend can be represented as a sum of the seasonal component ([O₃ SEASON]) and
575 long-term component ([O₃ LT]) trends. The spatial trend distributions of [O₃ BL] and its two
576 separated components of seasonal and long-term components are shown in Fig. 13. It is
577 noted that the period used in Fig. 13 is shorter than the total period of original data because
578 of truncation effect in the KZ-filter process. The long-term component obtained by the
579 KZ-filter of KZ_{365,3} loses 546 days at the beginning and end of original time series.

580 The increasing trends of O₃ are generally high in the SMA and southwestern part
581 and low in the southeastern coastal region of Korean peninsula (Fig. 13a). This spatial
582 inhomogeneity of the O₃ trends over South Korea is mainly contributed by the long-term
583 component trends (Fig. 13c) rather than the seasonal component trend (Fig. 13b).
584 Therefore, the large spatial variability in local precursor emissions induced the spatial
585 inhomogeneity of O₃ trends in South Korea. On the other hand, relatively homogeneous
586 distribution of the seasonal component trends implies that meteorological influences on the
587 long-term changes in O₃ have little regional dependence nationwide.

588 Since the spatially inhomogeneous O₃ trends are related to the local precursor
589 emissions, we also tried to investigate their relationship with NO₂ measurement data. To
590 detect temporally synchronous and spatially coupled patterns between the long-term
591 variations of O₃ and NO₂, we applied the SVD to [O₃ LT] and the long-term component of
592 NO₂ ([NO₂ LT]). [NO₂ LT] was simply obtained by applying the KZ-filter of KZ_{365,3} to the
593 log-transformed NO₂ time series. The SVD is usually applied to two combined space-time
594 data fields, based on the computation of a temporal cross-covariance matrix between two
595 data fields. The SVD identifies coupled spatial patterns and their temporal variations, with
596 each pair of spatial patterns explaining a fraction of the squared covariance between the
597 two space-time data sets. The squared covariance fraction (SCF) is largest in the first pair

598 (mode) of the patterns, and each succeeding mode has a maximum SCF that is unexplained
599 by the previous modes.

600 The first three leading SVD modes (singular vectors) of the coupled O₃ and NO₂
601 long-term components account for the SCF with 94.6% of the total, of which the first,
602 second, and third modes are 63.7%, 23.6%, and 7.3% respectively. Figure 14 displays the
603 expansion coefficients (coupled spatial patterns) and their time series of the first mode
604 along with spatial map of the [NO₂_{LT}] trends. The dominant first mode of the O₃ and NO₂
605 long-term components (Figs. 14a and 14b) is very similar to the spatial distributions of [O₃
606 _{LT}] trends (Fig. 13c) and [NO₂_{LT}] trends (Fig. 14c) respectively. In Fig. 14d, the strong
607 coherence in the time series is observed between the first modes of the [O₃_{LT}] and [NO₂
608 _{LT}] with a correlation coefficient of 0.98. The results of SVD analysis suggest that the
609 long-term variations of O₃ and NO₂ in South Korea have similar temporal evolutions with
610 different spatial patterns.

611 The differences in spatial patterns of [O₃_{LT}] and [NO₂_{LT}] as shown in Figs 14a
612 and 14b are required to be further investigated. Since the VOCs emissions from industry,
613 transportation, and the solvent usage in construction are large in South Korea (KMOE,
614 2013), further analyses of VOCs measurements are needed. On top of that, especially in
615 South Korea, biogenic precursor emissions are also potentially important for the analysis
616 due to dense urban vegetation in and around metropolitan areas. Therefore, there remains
617 the limitation of our current data analysis due to the lack of both VOC emission data and
618 observations of atmospheric concentrations of VOCs in South Korea.

619

620 **4. Conclusion**

621 This study has investigated various spatio-temporal features and inter-relationship
622 of surface O₃ and related meteorological variables over South Korea based on ground
623 measurements for the period 1999–2010. A general overview of surface O₃ in terms of
624 spatial distributions and its temporal trend is provided based on its decomposed
625 components by the KZ-filter.

626 In South Korea, the O₃ concentrations are low at the inland and SMA cities due to
627 the NO_x titration by anthropogenic emissions and high at the coastal cities possibly due to
628 the dynamic effects of the sea breeze. The averaged O₃ levels in South Korea have
629 increased for 1999–2010 with an averaged temporal linear trend of +0.26 ppbv yr⁻¹
630 (+1.15% yr⁻¹). The recent increase of the O₃ levels in East Asia may result from the recent

631 increase of anthropogenic precursor emissions and the long-term variations in
632 meteorological effects.

633 We applied a linear regression model to investigate the relationships between O₃
634 and meteorological variables such as temperature, insolation, dew-point temperature, sea-
635 level pressure, wind speed, and relative humidity. Spatial distribution of the R^2 values
636 shows high meteorological influences in the SMA and inland regions and low
637 meteorological influences in the coastal region. The high meteorological influences in the
638 SMA and inland regions are related to effective photochemical activity, which results from
639 large local precursor emissions and stagnant conditions with low wind speeds. On the
640 other hand, the low meteorological influences in the coastal region are related to large
641 transport effects of the background O₃ and ventilation and dry deposition with high wind
642 speeds.

643 In the SMA and inland region, the high O₃ probability ($O_{3\ 8h} > 60$ ppbv) increases
644 with the daily maximum temperature rise. Specifically in the SMA, the most populated
645 area in South Korea, the probability of the O₃ exceedances is almost doubled for about 4°C
646 increase in daily maximum temperature and reached 27% at 30°C. It is noted that the
647 variations in O₃ exceedance probabilities according to the maximum temperature show an
648 approximate logarithmic increase in the SMA and inland regions. It thus implies that these
649 regions will experience more frequent high O₃ events in the future climate conditions with
650 the increasing global temperature.

651 The O₃ time series observed at each monitoring site can be decomposed into the
652 short-term, seasonal, and long-term components by the KZ-filter. Relative contributions of
653 each separated component show that the short-term and seasonal variations account for
654 most of the O₃ variability. Relative contributions of the short-term component are large at
655 the coastal cities due to influence of the background O₃ transport. In contrast, those of the
656 seasonal component are large at the inland cities due to the high meteorological influences
657 on the O₃ variations.

658 The transport effects on the short-term component are shown in the probability
659 distributions of both high short-term component values and O₃ exceedances for each wind
660 direction. During the months of frequent high O₃ events (May–October) in South Korea,
661 the probabilities of both high short-term component O₃ and O₃ exceedances are higher in
662 the near-westerly wind condition rather than in other wind directions. For the short-term
663 time scale, the eastward long-range transport of O₃ and precursors from China can cause
664 the nationwide high probabilities of O₃ exceedances in the near-westerly wind condition.

665 However, the high probabilities of O₃ extreme events in downwind regions of the
666 thermoelectric power plants and industrial complexes are related to local transport of O₃
667 precursors which apparently enhances the O₃ levels.

668 The distribution of O₃ trends in South Korea is spatially inhomogeneous.
669 Although the relative contributions of the long-term components are much smaller than
670 those of other two components, such spatially inhomogeneous distribution of O₃ trend is
671 mainly contributed by the long-term component O₃ trends rather than the seasonal
672 component O₃ trend related to the long-term change of meteorological conditions. It is
673 because the long-term change of the local precursor emission has a localized effect on the
674 long-term O₃ change. SVD between O₃ and NO₂ shows that the long-term variations of O₃
675 and NO₂ in South Korea have similar temporal evolutions with different spatial patterns.
676 The results of SVD analysis clearly demonstrate the influences of local precursor
677 emissions on the long-term changes in O₃. However, the precise interpretation of the large
678 spatially inhomogeneous distribution in the long-term component O₃ trend is limited due
679 to lack of VOC measurements data.

680 The KZ-filter is a useful diagnostic tool to reveal the spatio-temporal features of
681 O₃ and its relationship with meteorological variables. General features revealed by the KZ-
682 filter analysis will provide a better understanding of spatial and temporal variations of
683 surface O₃ as well as possible influences of local emissions, transport, and climate change
684 on O₃ levels in South Korea. Our analyses would also be helpful as a reference for the
685 evaluation of chemistry transport models and furthermore for establishing appropriate O₃
686 control policy.

687

688 **Acknowledgements**

689 This study has been funded by the Green City Technology Flagship Program of the Korea
690 Institute of Science and Technology. Daeok Youn was supported by Chungbuk National
691 University. This work was done as Huikyo Lee's private venture and not in the author's
692 capacity as an employee of the Jet Propulsion Laboratory, California Institute of
693 Technology.

694

695 **References**

- 696 Akimoto, H.: Global air quality and pollution, *Science*, 302, 1716–1719,
697 doi:10.1126/science.1092666, 2003.
- 698 Bell, M. L., Goldberg, R., Hogrefe, C., Kinney, P. L., Knowlton, K., Lynn, B., Rosenthal,
699 J., Rosenzweig, C., and Patz., J. A.: Climate change, ambient ozone, and health in 50
700 US cities, *Climatic Change*, 82, 61–76, doi:10.1007/s10584-006-9166-7, 2007.
- 701 Bernard, S. M., Samet, J. M., Grambsch, A., Ebi, K. L., and Romieu, I.: The potential
702 impacts of climate variability and change on air pollution-related health effects in the
703 United States, *Environ. Health Persp.*, 109, 199–209, 2001.
- 704 Boo, K.-O., Kwon, W.-T., and Baek, H.-J.: Change of extreme events of temperature and
705 precipitation over Korea using regional projection of future climate change, *Geophys.*
706 *Res. Lett.*, 33, L01701, doi:10.1029/2005GL023378, 2006.
- 707 Camalier, L., Cox, W., and Dolwick, P.: The effects of meteorology on ozone in urban
708 areas and their use in assessing ozone trends, *Atmos. Environ.*, 41, 7127–7137, doi:
709 10.1016/j.atmosenv.2007.04.061, 2007.
- 710 Carmichael, G. R., Uno, I., Phadnis, M. J., Zhang, Y., and Sunwoo, Y.: Tropospheric
711 ozone production and transport in the springtime in East Asia, *J. Geophys. Res.*, 103,
712 10649–10671, doi:10.1029/97JD03740, 1998.
- 713 Chatani, S. and Sudo, K.: Influences of the variation in inflow to East Asia on surface
714 ozone over Japan during 1996-2005, *Atmos. Chem. Phys.*, 11, 8745–8758,
715 doi:10.5194/acp-11-8745-2011, 2011.
- 716 Dawson, J. P., Adams, P. J., and Pandis, S. N.: Sensitivity of ozone to summertime climate
717 in the eastern USA: A modeling case study, *Atmos. Environ.*, 41, 1494–1511,
718 doi:10.1016/j.atmosenv.2006.10.033, 2007.
- 719 Dibb, J. E., Talbot, R. W., Scheuer, E., Seid, G., DeBell, L., Lefer, B., and Ridley, B.:
720 Stratospheric influence on the northern North American free troposphere during
721 TOPSE: ⁷Be as a stratospheric tracer, *J. Geophys. Res.*, 108, 8363,
722 doi:10.1029/2001JD001347, 2003.
- 723 Diem, J. E.: A critical examination of ozone mapping from a spatial-scale perspective,
724 *Environ. Pollut.*, 125, 369–383, doi:10.1016/S0269-7491(03)00110-6, 2003.
- 725 Ding, A. J., Wang, T., Thouret, V., Cammas, J.-P., and Nédélec, P.: Tropospheric ozone
726 climatology over Beijing: analysis of aircraft data from the MOZAIC program,
727 *Atmos. Chem. Phys.*, 8, 1–13, doi:10.5194/acp-8-1-2008, 2008.

728 Eskridge, R. E., Ku, J. Y., Rao, S. T., Porter, P. S., and Zurbenko, I. G.: Separating
729 different scales of motion in time series of meteorological
730 variables, *B. Am. Meteorol. Soc.*, 78, 1473–1483, doi:10.1175/1520-
731 0477(1997)078<1473:SDSOMI>2.0.CO;2, 1997.

732 Flaum, J. B., Rao, S. T., and Zurbenko, I. G.: Moderating the influence of meteorological
733 conditions on ambient ozone concentrations, *J. Air Waste Manage.*, 46, 35–46,
734 doi:10.1080/10473289.1996.10467439, 1996.

735 Gardner, M. W. and Dorling, S. R.: Meteorologically adjusted trends in UK daily
736 maximum surface ozone concentrations, *Atmos. Environ.*, 34, 171–176,
737 doi:10.1016/S1352-2310(99)00315-5, 2000.

738 Ghim, Y. S.: Trends and factors of ozone concentration variations in Korea, *Journal of*
739 *Korean Society for Atmospheric Environment*, 16, 607–623, 2000. (In Korean)

740 Ghim, Y. S. and Chang, Y. S.: Characteristics of ground-level ozone distribution in Korea
741 for the period of 1990-1995, *J. Geophys. Res.*, 105, 8877–8890,
742 doi:10.1029/1999JD901179, 2000.

743 Ghim, Y. S., Oh, H. S., and Chang, Y. S.: Meteorological effects on the evolution of high
744 ozone episodes in the Greater Seoul Area, *J. Air Waste Manage.*, 51, 185–202,
745 doi:10.1080/10473289.2001.10464269, 2001.

746 Guicherit, R. and Roemer, M.: Tropospheric ozone trends, *Chemosphere-Global Change*
747 *Science*, 2, 167–183, 2000.

748 Ibarra-Berastegi, G., Madariaga, I., Elías, A., Agirre, E., and Uria, J.: Long-term changes
749 of ozone and traffic in Bilbao, *Atmos. Environ.*, 35, 5581–5592, doi:10.1016/S1352-
750 2310(01)00210-2, 2001.

751 IPCC (Intergovernmental Panel on Climate Change): *Climate Change 2007: The Physical*
752 *Scientific Basis: Contribution of Working Group I to the Fourth Assessment Report*
753 *of the Intergovernmental Panel on Climate Change*, edited by: Solomon, S., Qin, D.,
754 Manning, M., Chen, Z., Marquis, M., Averyt, K. B., Tignor, M., and Miller, H. L.,
755 Cambridge University Press, Cambridge, United Kingdom and New York, NY, USA,
756 2007.

757 Jacob, D. J., Logan, J. A., and Murti, P. P.: Effect of rising Asian emissions on surface
758 ozone in the United States, *Geophys. Res. Lett.*, 26, 2175–2178,
759 doi:10.1029/1999GL900450, 1999.

760 Jacob, D. J. and Winner, D. A.: Effect of climate change on air quality, *Atmos. Environ.*,
761 43, 51–63, doi:10.1016/j.atmosenv.2008.09.051, 2009.

762 Jaffe, D. A., Parrish, D., Goldstein, A., Price, H., and Harris, J.: Increasing background
763 ozone during spring on the west coast of North America, *J. Geophys. Res.*, 30, 1613,
764 doi:10.1029/2003GL017024, 2003.

765 Jin, L., Lee, S.-H., Shin, H.-J., and Kim, Y. P.: A study on the ozone control strategy using
766 the OZIPR in the Seoul Metropolitan Area, *Asian J. Atmos. Environ.*, 6, 111–117,
767 doi:10.5572/ajae.2012.6.2.111, 2012.

768 Kim, J. Y., Kim, S.-W., Ghim, Y. S., Song, C. H., and Yoon, S.-C.: Aerosol properties at
769 Gosan in Korea during two pollution episodes caused by contrasting weather
770 conditions, *Asia-Pacific J. Atmos. Sci.*, 48(1), 25–33, doi:10.1007/s13143-012-0003-
771 9, 2012.

772 KMOE (Ministry of Environment, Korea): Annual report of ambient air quality in Korea,
773 2011, 11-1480523-000198-10, National Institute of Environmental Research,
774 Environmental Research Complex, Incheon, 2012. (In Korean, available at:
775 <http://webbook.me.go.kr/DLi-File/091/012/5515496.PDF>)

776 KMOE (Ministry of Environment, Korea): Air pollutants emission (1999–2010), 11-
777 1480523-001377-01, National Institute of Environmental Research, Environmental
778 Research Complex, Incheon, 2013. (In Korean, available at:
779 <http://webbook.me.go.kr/DLi-File/NIER/09/018/5553596.pdf>)

780 Lei, H., Wuebbles, D. J., Liang, X.-Z., and Olsen, S.: Domestic versus international
781 contributions on 2050 ozone air quality: How much is convertible by regional
782 control?, *Atmos. Environ.*, 68, 315–325, doi:10.1016/j.atmosenv.2012.12.002, 2013.

783 Lei, H. and Wang, J. X. L.: Sensitivities of NO_x transformation and the effects on surface
784 ozone and nitrate, *Atmos. Chem. Phys.*, 14, 1385–1396, doi:10.5194/acp-14-1385-
785 2014, 2014.

786 Levy, H., Mahlman, J., Moxim, W. J., and Liu, S.: Tropospheric ozone: the role of
787 transport, *J. Geophys. Res.*, 90, 3753–3772, doi:10.1029/JD090iD02p03753, 1985.

788 Levy, J. I., Chemerynski, S. M., and Sarnat, J. A.: Ozone exposure and mortality: an
789 empiric Bayes metaregression analysis, *Epidemiology*, 16, 458–468, doi:
790 10.1097/01.ede.0000165820.08301.b3, 2005.

791 Lin, C. Y. C., Jacob, D. J., and Fiore, A. M.: Trends in exceedances of the ozone air
792 quality standard in the continental United States, 1980-1998, *Atmos. Environ.*, 35,
793 3217–3228, doi:10.1016/S1352-2310(01)00152-2, 2001.

794 Lin, J.-T., Patten, K. O., Hayhoe, K., Liang, X.-Z., and Wuebbles, D. J.: Effects of future
795 climate and biogenic emissions changes on surface ozone over the United States and

796 China, *J. Appl. Meteorol. Clim.*, 47, 1888–1909, doi:10.1175/2007JAMC1681.1,
797 2008.

798 Liu, S. C., Trainer, M., Fehsenfeld, F. C., Parrish, D. D., Williams, E. J., Fahey, D. W.,
799 Hübler, G., and Murphy, P. C.: Ozone production in the rural troposphere and the
800 implications for regional and global ozone distributions, *J. Geophys. Res.*, 92, D4,
801 4191–4207, doi:10.1029/JD092iD04p04191, 1987.

802 Logan, J. A.: Tropospheric ozone: seasonal behavior, trends and anthropogenic influence,
803 *J. Geophys. Res.*, 90, 463–482, doi:10.1029/JD090iD06p10463, 1985.

804 Lu, H. C. and Chang, T. S.: Meteorologically adjusted trends of daily maximum ozone
805 concentrations in Taipei, Taiwan, *Atmos. Environ.*, 39, 6491–6501,
806 doi:10.1016/j.atmosenv.2005.06.007, 2005.

807 Lu, G. Y. and Wong, D. W.: An adaptive inverse-distance weighting spatial interpolation
808 technique, *Comput. Geosci.*, 34, 1044–1055, doi:10.1016/j.cageo.2007.07.010, 2008.

809 Mickley, L. J., Jacob, D. J., and Field, B. D.: Climate response to the increase in
810 tropospheric ozone since preindustrial times: A comparison between ozone and
811 equivalent CO₂ forcings, *J. Geophys. Res.*, 109, D05106, doi:10.1029/2003JD003653,
812 2004.

813 Milanchus, M. L., Rao, S. T., and Zurbenko, I. G.: Evaluating the effectiveness of ozone
814 management efforts in the presence of meteorological variability, *J. Air Waste*
815 *Manage.*, 48, 201–215, doi:10.1080/10473289.1998.10463673, 1998.

816 Nagashima, T., Ohara, T., Sudo, K., and Akimoto, H.: The relative importance of various
817 source regions on East Asian surface ozone, *Atmos. Chem. Phys.*, 10, 11305–11322,
818 doi:10.5194/acp-10-11305-2010, 2010.

819 Oh, I. B., Kim, Y. K., Lee, H. W., and Kim, C. H.: An observational and numerical study
820 of the effects of the late sea breeze on ozone distributions in the Busan metropolitan
821 area, Korea, *Atmos. Environ.*, 40, 1284–1298, doi:10.1016/j.atmosenv.2005.10.049,
822 2006.

823 Oh, I. B., Kim, Y. K., Hwang, M. K., Kim, C. H., Kim, S., and Song, S. K.: Elevated
824 ozone layers over the Seoul Metropolitan Region in Korea: Evidence for long-range
825 ozone transport from eastern China and its contribution to surface concentrations, *J.*
826 *Appl. Meteorol. Clim.*, 49, 203–220, doi:10.1175/2009JAMC2213.1, 2010.

827 Olszyna, K. J., Luria, M., and Meagher, J. F.: The correlation of temperature and rural
828 ozone levels in southeastern U.S.A., *Atmos. Environ.*, 31, 3011–3022,
829 doi:10.1016/S1352-2310(97)00097-6, 1997.

830 Oltmans, S. J., Lefohn, A. S., Scheel, H. E., Harris, J. M., Levy II, H., Galbally, I. E.,
831 Brunke, E.-G., Meyer, C. P., Lathrop, J. A., Johnson, B. J., Shadwick, D. S., Cuevas,
832 E., Schmidlin, F. J., Tarasick, D. W., Claude, H., Kerr, J. B., Uchino, O., and Mohnen,
833 V.: Trends of ozone in the troposphere, *Geophys. Res. Lett.*, 25, 139–142,
834 doi:10.1029/97GL03505, 1998.

835 Oltmans, S. J., Lefohn, A. S., Harris, J. M., Galbally, I., Scheel, H. E., Bodeker, G.,
836 Brunke, E., Claude, H., Tarasick, D., Johnson, B. J., Simmonds, P., Shadwick, D.,
837 Anlauf, K., Hayden, K., Schmidlin, F., Fujimoto, T., Akagi, K., Meyer, C., Nichol, S.,
838 Davies, J., Redondas, A., and Cuevas, E.: Long-term changes in tropospheric ozone,
839 *Atmos. Environ.*, 40, 3156–3173, doi:10.1016/j.atmosenv.2006.01.029, 2006.

840 Oltmans, S. J., Lefohn, A. S., Shadwick, D., Harris, J. M., Scheel, H. E., Galbally, I.,
841 Tarasick, D. W., Johnson, B. J., Brunke, E.-G., Claude, H., Zeng, G., Nichol, S.,
842 Schmidlin, F., Davies, J., Cuevas, E., Redondas, A., Naoe, H., Nakano, T., and
843 Kawasato, T.: Recent tropospheric ozone changes – A pattern dominated by slow or
844 no growth, *Atmos. Environ.*, 67, 331–351, doi:10.1016/j.atmosenv.2012.10.057, 2013.

845 Ordóñez, C., Mathis, H., Furger, M., Henne, S., Hüglin, C., Staehelin, J., and Prévôt, A. S.
846 H.: Changes of daily surface ozone maxima in Switzerland in all seasons from 1992
847 to 2002 and discussion of summer 2003, *Atmos. Chem. Phys.*, 5, 1187–1203,
848 doi:10.5194/acp-5-1187-2005, 2005.

849 Racherla, P. N. and Adams, P. J.: Sensitivity of global tropospheric ozone and fine
850 particulate matter concentrations to climate change, *J. Geophys. Res.*, 111, D24103,
851 doi:10.1029/2005JD006939, 2006.

852 Rao, S. T. and Zurbenko, I. G.: Detecting and tracking changes in ozone air quality, *J. Air*
853 *Waste Manage.*, 44, 1089–1092, doi:10.1080/10473289.1994.10467303, 1994.

854 Rao, S. T., Zalewsky, E., and Zurbenko, I. G.: Determining temporal and spatial variations
855 in ozone air quality, *J. Air Waste Manage.*, 45, 57–61,
856 doi:10.1080/10473289.1995.10467342, 1995.

857 Rao, S. T., Zurbenko, I. G., Neagu, R., Porter, P. S., Ku, J. Y., and Henry, R. F.: Space and
858 time scales in ambient ozone data, *B. Am. Meteorol. Soc.*, 78, 2153–2166,
859 doi:10.1175/1520-0477(1997)078<2153:SATSIA>2.0.CO;2, 1997.

860 Rasmussen, D. J., Fiore, A. M., Naik, V., Horowitz, L. W., McGinnis, S. J., and Schultz,
861 M. G.: Surface ozone-temperature relationships in the eastern US: A monthly
862 climatology for evaluating chemistry-climate models, *Atmos. Environ.*, 47, 142–153,
863 doi:10.1016/j.atmosenv.2011.11.021, 2012.

864 Shin, H. J., Cho, K. M., Han, J. S., Kim, J. S., and Kim, Y. P.: The effects of precursor
865 emission and background concentration changes on the surface ozone concentration
866 over Korea, *Aerosol Air Qual. Res.*, 12, 93–103, doi:10.4209/aaqr.2011.09.0141,
867 2012.

868 Sillman, S. and Samson, P. J.: Impact of temperature on oxidant photochemistry in urban,
869 polluted rural and remote environments, *J. Geophys. Res.*, 100, 11497–11508,
870 doi:10.1029/94JD02146, 1995.

871 Tang, G., Wang, Y., Xin, J., and Ren, X.: Surface ozone trend details and interpretations in
872 Beijing, 2001–2006, *Atmos. Chem. Phys.*, 9, 8813–8823, doi:10.5194/acp-9-8813-
873 2009, 2009.

874 Tanimoto, H., Sawa, Y., Matsueda, H., Uno, I., Ohara, T., Yamaji, K., Kurokawa, J., and
875 Yonemura, S.: Significant latitudinal gradient in the surface ozone spring maximum
876 over East Asia, *Geophys. Res. Lett.*, 32, L21805, doi:10.1029/2005GL023514, 2005.

877 Tanimoto, H., Ohara, T., and Uno, I.: Asian anthropogenic emissions and decadal trends in
878 springtime tropospheric ozone over Japan: 1998–2007, *Geophys. Res. Lett.*, 36,
879 L23802, doi:10.1029/2009GL041382, 2009.

880 Thompson, M. L., Reynolds, J. R., Cox, L. H., Guttorp, P., and Sampson, P. D.: A review
881 of statistical methods for the meteorological adjustment of tropospheric ozone, *Atmos.*
882 *Environ.*, 35, 617–630, doi:10.1016/S1352-2310(00)00261-2, 2001.

883 Tilmes, S. and Zimmermann, J.: Investigation on the spatial scales of the variability in
884 measured near-ground ozone mixing ratios, *Geophys. Res. Lett.*, 25, 3827–3830,
885 doi:10.1029/1998GL900034, 1998.

886 Tsakiri, K. G. and Zurbenko, I. G.: Prediction of ozone concentrations using atmospheric
887 variables, *Air Quality, Atmosphere & Health*, 4, 111–120, doi:10.1007/s11869-010-
888 0084-5, 2011.

889 Vingarzan, R.: A review of surface ozone background levels and trends, *Atmos. Environ.*,
890 38, 3431–3442, doi:10.1016/j.atmosenv.2004.03.030, 2004.

891 Wang, T., Wei, X. L., Ding, A. J., Poon, C. N., Lam, K. S., Li, Y. S., Chan, L. Y., and
892 Anson, M.: Increasing surface ozone concentrations in the background atmosphere of
893 Southern China, 1994–2007, *Atmos. Chem. Phys.*, 9, 6217–6227, doi:10.5194/acp-9-
894 6217-2009, 2009.

895 Wang, X. and Mauzerall, D. L.: Characterizing distributions of surface ozone and its
896 impact on grain production in China, Japan and South Korea: 1990 and 2020, *Atmos.*
897 *Environ.*, 38, 4383–4402, doi:10.1016/j.atmosenv.2004.03.067, 2004.

898 Wang, Y., Konopka, P., Liu, Y., Chen, H., Müller, R., Plöger, F., Riese, M., Cai, Z., and
899 Lü, D.: Tropospheric ozone trend over Beijing from 2002–2010: ozonesonde
900 measurements and modeling analysis, *Atmos. Chem. Phys.*, 12, 8389–8399,
901 doi:10.5194/acp-12-8389-2012, 2012.

902 Wise, E. K. and Comrie, A. C.: Extending the Kolmogorov-Zurbenko filter: Application to
903 ozone, particulate matter, and meteorological trends, *J. Air Waste Manage.*, 55, 1208–
904 1216, doi:10.1080/10473289.2005.10464718, 2005.

905 Zhao, B., Wang, S. X., Liu, H., Xu, J. Y., Fu, K., Klimont, Z., Hao, J. M., He, K. B.,
906 Cofala, J., and Amann, M.: NO_x emissions in China: historical trends and future
907 perspectives, *Atmos. Chem. Phys.*, 13, 9869–9897, doi:10.5194/acp-13-9869-2013,
908 2013.

909

910 Table and Figure captions

911 Table 1. 12-yr averaged concentrations and temporal linear trends of daily average O_3 ($O_{3\text{ avg}}$) at 46
912 cities over South Korea for the period 1999–2010. The cities are categorized into three
913 groups: 16 coastal cities, 14 inland cities, and 16 cities in the Seoul Metropolitan Area
914 (SMA).

915 Table 2. Coefficients of determination (R^2) between baseline of daily maximum 8-h average O_3 ($O_{3\text{ 8h}}$)
916 and baselines of six meteorological variables (T_{max} , SI, TD, PS, WS, and RH) at 25 cities
917 over South Korea for the period 1999–2010. Adjusted R^2 ($Adj. R^2$) between baseline of $O_{3\text{ 8h}}$
918 and combined meteorological effects ($a_0 + \sum_i a_i MET_{BL}(t)_i$) are also represented. The cities
919 are categorized into three groups: 10 coastal cities, 11 inland cities, and 4 cities in the Seoul
920 Metropolitan Area (SMA). Numbers in bold fonts indicate correlations significant at the
921 95% level or higher.

922 Table 3. 12-yr averaged of daily minimum O_3 ($O_{3\text{ min}}$) concentrations and daily average wind
923 speeds (WS) at 46 cities over South Korea for the period 1999–2010. The cities are
924 categorized into three groups: 16 coastal cities, 14 inland cities, and 16 cities in the Seoul
925 Metropolitan Area (SMA).

926 Table 4. Relative contributions (%) of short-term components ($[O_{3\text{ ST}}]$), seasonal components ($[O_{3\text{ SEASON}}]$),
927 and long-term components ($[O_{3\text{ LT}}]$) to total variance of log-transformed daily
928 maximum 8-h average O_3 ($[O_3]$) at 25 cities over South Korea for the period 1999–2010.
929 The cities are categorized into three groups: 10 coastal cities, 11 inland cities, and 4 cities in
930 the Seoul Metropolitan Area (SMA).

931 Figure 1. (a) Geographical locations of South Korea, and (b) 72 weather stations of the Korea
932 Meteorological Administration (KMA) with blue circles, (c) 124 air quality monitoring sites
933 of the National Institute of Environmental Research (NIER) with black dots, and (d) 72 air
934 quality monitoring sites of NIER, which are located within 10 km from 25 weather stations
935 of KMA over the South Korean domain.

936 Figure 2. Time series of daily maximum 8-h average ozone ($O_{3\text{ 8h}}$) at the City Hall of Seoul and its
937 separated components such as (a) log-transformed $O_{3\text{ 8h}}$ time series ($[O_3]$) and its baseline
938 ($[O_{3\text{ BL}}]$), (b) short-term component ($[O_{3\text{ ST}}]$), (c) seasonal component ($[O_{3\text{ SEASON}}]$), and (d)
939 long-term component ($[O_{3\text{ LT}}]$) by applying KZ-filter. It is noted that the longer window
940 length causes the larger truncation of the result (Wise and Comrie, 2005) since the KZ-filter
941 is an iterative moving average process. The baseline in red solid line is superimposed in (a).

942 Figure 3. Spatial distributions of 12-yr averaged concentrations of (a) daily average O_3 ($O_{3\text{ avg}}$) and
943 (b) daily average nitrogen dioxide ($NO_{2\text{ avg}}$), and (c) temporal linear trends of $O_{3\text{ avg}}$ for the
944 period 1999–2010 using data from 124 air quality monitoring sites (black dots) of NIER.

945 Figure 4. Spatial distributions of temporal linear trends of (a) daily average temperature (T) and (b)
946 daily average surface insolation (SI) for the period 1999–2010 using data from 72 and 22
947 weather stations (black dots) of KMA, respectively.

948 Figure 5. Spatial distributions of squared correlation coefficients (R^2) between baselines of $O_{3\text{ 8h}}$
949 ($[O_{3\text{ BL}}]$) and (a) daily maximum temperature ($T_{\text{max BL}}$) and (b) surface insolation ($SI_{\text{ BL}}$).
950 Black dots represent 72 air quality monitoring sites of NIER. (c) Spatial distribution of
951 adjusted R^2 between $[O_{3\text{ BL}}]$ and combined meteorological effects ($a_0 + \sum_i a_i MET_{BL}(t)_i$).

952 Figure 6. (a) Spatial distribution of 12-yr averaged concentrations of daily minimum O_3 ($O_{3\ min}$) for
953 the period 1999–2010 using data from 124 air quality monitoring sites (black dots) of NIER.
954 (b) Scatter plot of R^2 between $[O_{3\ BL}]$ and $T_{\max\ BL}$ versus $O_{3\ min}$ at 25 cities. (c) Scatter plot of
955 R^2 between $[O_{3\ BL}]$ and SI_{BL} versus $O_{3\ min}$ at 17 cities. City codes in red, green, and blue
956 indicate the Seoul Metropolitan Area (SMA), inland, and coastal cities, respectively.

957 Figure 7. (a) Spatial distribution of 12-yr averaged daily average wind speeds (WS) for the period
958 1999–2010 using data from 72 weather stations (black dots) of KMA. (b) Scatter plot of $O_{3\ min}$
959 versus WS at 25 cities. (c) Scatter plot of R^2 between $[O_{3\ BL}]$ and $T_{\max\ BL}$ versus WS at 25
960 cities. City codes in red, green, and blue indicate the Seoul Metropolitan Area (SMA),
961 inland, and coastal cities, respectively.

962 Figure 8. Probabilities of O_3 exceedances in the given range of daily maximum temperature (T_{\max})
963 that $O_{3\ 8h}$ will exceed air quality standard of South Korea (60 ppbv).

964 Figure 9. Spatial distributions of relative contributions of (a) short-term component ($[O_{3\ ST}]$), (b)
965 seasonal component ($[O_{3\ SEASON}]$), and (c) long-term component ($[O_{3\ LT}]$) to the total
966 variance of original time series ($[O_3]$) using data from 72 air quality monitoring sites (black
967 dots) of NIER. Note that the color scales are all different.

968 Figure 10. Relationships between wind directions (WD) and exponentials of short-term
969 components ($\exp[O_{3\ ST}]$) during the months of frequent high O_3 events (May–October) at
970 Seoul (a–b), Incheon (c–d), Suwon (e–f), and Ganghwa (g–h) in the Seoul Metropolitan
971 Area (SMA) are represented in scatter plots of $\exp[O_{3\ ST}]$ versus WD (a, c, e, and g) and
972 probabilities of O_3 exceedances in each WD (b, d, f, and h). Red dots in scatter plots denote
973 high O_3 episodes that daily maximum 8-h average O_3 ($O_{3\ 8h}$) will exceed air quality
974 standard of South Korea (60 ppbv). Dashed lines in scatter plots denote the reference of $\exp[O_{3\ ST}] =$
975 1. Probabilities of $\exp[O_{3\ ST}] > 1$ and $O_{3\ 8h} > 60$ ppbv in each WD are represented as black
976 thick lines and red thick lines, respectively. 95% of confidence intervals for each probability
977 are represented as black and red thin lines. We used O_3 data from 12 sites in Seoul, 6 sites
978 in Incheon, 3 sites in Suwon, and 1 site in Ganghwa.

979 Figure 11. Spatial distributions of probabilities that exponentials of the short-term components will
980 exceed 1 ($\exp[O_{3\ ST}] > 1$) for each wind direction (WD) of (a) northerly (N), (b)
981 northeasterly (NE), (c) easterly (E), (d) southeasterly (SE), (e) southerly (S), (f)
982 southwesterly (SW), (g) westerly (W), and (h) northwesterly (NW), respectively. Black dots
983 denote 25 weather stations of KMA and triangles denote 26 major thermoelectric power
984 plants in South Korea (blue triangle < 1000 MW, red triangles ≥ 1000 MW).

985 Figure 12. Spatial distributions of probabilities that daily maximum 8-h average O_3 ($O_{3\ 8h}$) will
986 exceed air quality standard of South Korea (60 ppbv) for each wind direction (WD) of (a)
987 northerly (N), (b) northeasterly (NE), (c) easterly (E), (d) southeasterly (SE), (e) southerly
988 (S), (f) southwesterly (SW), (g) westerly (W), and (h) northwesterly (NW), respectively.
989 Black dots denote 25 weather stations of KMA and triangles denote 26 major thermoelectric
990 power plants in South Korea (blue triangle < 1000 MW, red triangles ≥ 1000 MW).

991 Figure 13. Spatial distributions of temporal linear trends of (a) baseline ($[O_{3\ BL}]$), (b) seasonal
992 component ($[O_{3\ SEASON}]$), and (c) long-term component ($[O_{3\ LT}]$) for the period 2000–2009
993 using data from 72 air quality monitoring sites of NIER.

994 Figure 14. The first leading mode of SVD between the long-term components of (a) daily
995 maximum 8-h average O_3 ($[O_{3\ LT}]$) and (b) daily average NO_2 ($[NO_{2\ LT}]$) for the period 2000–

996 2009. (c) Spatial distribution of temporal linear trends of $[\text{NO}_{2\text{LT}}]$. (d) Time series of the
997 SVD expansion coefficient associated with $[\text{O}_{3\text{LT}}]$ mode (blue line) and $[\text{NO}_{2\text{LT}}]$ mode (red
998 line).

Table 1. 12-yr averaged concentrations and temporal linear trends of daily average O₃ (O_{3 avg}) at 46 cities over South Korea for the period 1999–2010. The cities are categorized into three groups: 16 coastal cities, 14 inland cities, and 16 cities in the Seoul Metropolitan Area (SMA).

Coastal region	City code	O _{3 avg} (ppbv)	Trend (% yr ⁻¹)	Inland region	City code	O _{3 avg} (ppbv)	Trend (% yr ⁻¹)	SMA	City code	O _{3 avg} (ppbv)	Trend (% yr ⁻¹)
Busan*	BS	23.2	0.65	Andong	AD	22.0	1.35	Ansan	-	20.5	1.81
Changwon	CW	25.1	1.62	Cheonan	CN	18.7	0.72	Anyang	-	16.8	0.67
Gangneung	GN	26.5	2.61	Cheongju	CJ	21.0	1.25	Bucheon	-	18.3	1.71
Gimhae	-	24.4	-0.05	Daegu*	DG	19.8	0.77	Ganghwa	GH	30.9	1.12
Gunsan	GS	22.5	0.66	Daejeon*	DJ	20.7	1.21	Goyang	-	19.1	0.77
Gwangyang	-	28.1	-1.28	Gimcheon	-	24.4	2.36	Gunpo	-	19.6	-0.86
Jeju	JJ1	32.6	2.59	Gumi	GM	22.6	3.70	Guri	-	18.1	-0.83
Jinhae	-	31.3	1.03	Gwangju*	GJ	20.5	3.50	Gwacheon	-	17.6	-1.25
Masan	-	25.2	0.85	Gyeongju	-	22.1	-0.27	Gwangmyeong	-	18.0	0.41
Mokpo	MP	30.3	-0.21	Iksan	-	17.7	2.64	Incheon*	IC	19.0	1.45
Pohang	PH	25.7	0.01	Jecheon	JC	21.0	-0.21	Pyeongtaek	-	19.9	2.75
Seosan	SS	27.5	-1.67	Jeonju	JJ2	18.9	2.55	Seongnam	-	18.8	0.66
Suncheon	-	25.7	0.92	Jinju	JJ3	24.0	2.54	Seoul*	SU	17.1	2.82
Ulsan*	US	21.5	1.61	Wonju	WJ	20.7	-0.24	Siheung	-	21.0	2.29
Yeongam	-	28.6	3.58					Suwon	SW	19.3	1.86
Yeosu	YS	28.1	1.18					Uijeongbu	-	19.9	1.46
Coastal averages		26.6	0.88	Inland averages		21.0	1.56	SMA averages		19.6	1.05
Nationwide averages		22.5	1.15								

* : Major metropolitan cities in South Korea (Seoul, Busan, Daegu, Incheon, Gwangju, Daejeon, and Ulsan)

Table 2. Coefficients of determination (R^2) between baseline of daily maximum 8-h average O_3 ($O_{3\ 8h}$) and baselines of six meteorological variables (T_{\max} , SI, TD, PS, WS, and RH) at 25 cities over South Korea for the period 1999–2010. Adjusted R^2 ($Adj. R^2$) between baseline of $O_{3\ 8h}$ and combined meteorological effects ($a_0 + \sum_i a_i MET_{BL}(t)_i$) are also represented. The cities are categorized into three groups: 10 coastal cities, 11 inland cities, and 4 cities in the Seoul Metropolitan Area (SMA). Numbers in bold fonts indicate correlations significant at the 95% level or higher.

	Cities	City code	Coefficients of determination (R^2)						$Adj. R^2$
			T_{\max}	SI	TD	PS	WS	RH	
Coastal region	Busan ¹	BS	0.147	0.366	0.139	0.222 ²	0.014	0.135	0.408
	Changwon	CW	0.224	n/a	0.179	0.335 ²	0.001 ²	0.138	0.533
	Gangneung	GN	0.013	0.480	0.000	0.072 ²	0.014	0.008 ²	0.449
	Gunsan	GS	0.032	n/a	0.017	0.047 ²	0.002	0.003 ²	0.164
	Jeju	JJ1	0.028 ²	0.080	0.069 ²	0.004	0.009	0.141 ²	0.337
	Mokpo	MP	0.012	0.263	0.004	0.038 ²	0.047 ²	0.043 ²	0.427
	Pohang	PH	0.034	0.404	0.014	0.102 ²	0.043 ²	0.003	0.398
	Seosan	SS	0.059	0.495	0.021	0.135 ²	0.001	0.049 ²	0.506
	Ulsan ¹	US	0.071	n/a	0.046	0.107 ²	0.035 ²	0.023	0.186
	Yeosu	YS	0.093	n/a	0.061	0.140 ²	0.002 ²	0.024	0.251
Averages			0.071	0.348	0.055	0.120 ²	0.017	0.057	0.366
Inland region	Andong	AD	0.269	0.544	0.128	0.379 ²	0.004	0.026 ²	0.628
	Cheonan	CN	0.400	n/a	0.263	0.479 ²	0.003 ²	0.056 ²	0.674
	Cheongju	CJ	0.387	0.666	0.219	0.443 ²	0.052	0.053 ²	0.674
	Daegu ¹	DG	0.381	0.621	0.224	0.493 ²	0.002 ²	0.016	0.703
	Daejeon ¹	DJ	0.312	0.721	0.160	0.408 ²	0.089	0.062 ²	0.724
	Gumi	GM	0.244	n/a	0.116	0.361 ²	0.009 ²	0.038 ²	0.563
	Gwangju ¹	GJ	0.274	0.502	0.159	0.315 ²	0.015	0.005 ²	0.570
	Jecheon	JC	0.258	n/a	0.137	0.365 ²	0.012	0.108 ²	0.589
	Jeonju	JJ2	0.134	0.434	0.060	0.179 ²	0.008 ²	0.038 ²	0.404
	Jinju	JJ3	0.199	0.413	0.129	0.238 ²	0.000	0.012	0.396
Wonju	WJ	0.476	0.767	0.312	0.573 ²	0.069	0.018 ²	0.799	
Averages			0.303	0.584	0.173	0.385 ²	0.024	0.039 ²	0.611
SMA	Ganghwa	GH	0.204	n/a	0.158	0.274 ²	0.190	0.025	0.389
	Incheon ¹	IC	0.310	0.501	0.250	0.411 ²	0.019 ²	0.097	0.577
	Seoul ¹	SU	0.419	0.580	0.318	0.531 ²	0.009 ²	0.045	0.693
	Suwon	SW	0.525	0.703	0.422	0.640 ²	0.009	0.080	0.818
Averages			0.364	0.595	0.287	0.464 ²	0.057	0.062	0.619
Nationwide averages			0.220	0.502	0.144	0.292 ²	0.026	0.050 ²	0.514

¹ : Major metropolitan cities in South Korea

² : Negative correlation

n/a: Not available observations of SI

MET_{BL} : Combined meteorological variables regressed on $[O_{3\ BL}]$ ($a_0 + \sum_i a_i MET_{BL}(t)_i$)

Table 3. 12-yr averaged of daily minimum O₃ (O_{3 min}) concentrations and daily average wind speeds (WS) at 46 cities over South Korea for the period 1999–2010. The cities are categorized into three groups: 16 coastal cities, 14 inland cities, and 16 cities in the Seoul Metropolitan Area (SMA).

Coastal region	City code	O _{3 min} (ppbv)	WS (m s ⁻¹)	Inland region	City code	O _{3 min} (ppbv)	WS (m s ⁻¹)	SMA	City code	O _{3 min} (ppbv)	WS (m s ⁻¹)
Busan*	BS	8.2	3.38	Andong	AD	5.6	1.61	Ansan	-	5.7	n/a
Changwon	CW	7.9	2.01	Cheonan	CN	4.9	1.79	Anyang	-	3.9	n/a
Gangneung	GN	11.1	2.86	Cheongju	CJ	6.0	1.70	Bucheon	-	5.9	n/a
Gimhae	-	7.7	n/a	Daegu*	DG	5.6	2.31	Ganghwa	GH	12.9	1.84
Gunsan	GS	8.8	3.07	Daejeon*	DJ	5.7	1.96	Goyang	-	6.2	n/a
Gwangyang	-	12.9	n/a	Gimcheon	-	7.9	n/a	Gunpo	-	4.8	n/a
Jeju	JJ1	15.4	3.31	Gumi	GM	7.1	1.53	Guri	-	4.4	n/a
Jinhae	-	13.3	n/a	Gwangju*	GJ	6.0	2.07	Gwacheon	-	4.8	n/a
Masan	-	8.6	n/a	Gyeongju	-	7.9	n/a	Gwangmyeong	-	5.6	n/a
Mokpo	MP	14.1	3.64	Iksan	-	6.4	n/a	Incheon*	IC	5.2	2.69
Pohang	PH	11.5	2.68	Jecheon	JC	6.1	1.51	Pyeongtaek	-	4.9	n/a
Seosan	SS	12.3	2.66	Jeonju	JJ2	6.5	2.02	Seongnam	-	5.8	n/a
Suncheon	-	9.4	1.16	Jinju	JJ3	8.2	1.37	Seoul*	SU	3.8	2.27
Ulsan*	US	7.5	2.12	Wonju	WJ	5.9	1.09	Siheung	-	6.6	n/a
Yeongam	-	13.7	n/a					Suwon	SW	5.2	1.86
Yeosu	YS	11.5	4.30					Uijeongbu	-	4.9	n/a
Coastal averages		10.9	2.84	Inland averages		6.4	1.72	SMA averages		5.6	2.17
Nationwide averages		7.7	2.26								

* : Major metropolitan cities in South Korea

n/a: Not available observations of wind speed

Table 4. Relative contributions (%) of short-term components ($[O_3]_{ST}$), seasonal components ($[O_3]_{SEASON}$), and long-term components ($[O_3]_{LT}$) to total variance of log-transformed daily maximum 8-h average O_3 ($[O_3]$) at 25 cities over South Korea for the period 1999–2010. The cities are categorized into three groups: 10 coastal cities, 11 inland cities, and 4 cities in the Seoul Metropolitan Area (SMA).

Coastal region	City code	Relative contributions (%)			Inland region	City code	Relative contributions (%)			SMA	City code	Relative contributions (%)		
		$[O_3]_{ST}$	$[O_3]_{SEASON}$	$[O_3]_{LT}$			$[O_3]_{ST}$	$[O_3]_{SEASON}$	$[O_3]_{LT}$			$[O_3]_{ST}$	$[O_3]_{SEASON}$	$[O_3]_{LT}$
Busan*	BS	56.1	32.6	2.5	Andong	AD	32.7	53.2	3.6	Ganghwa	GH	56.2	33.1	3.2
Changwon	CW	53.6	36.2	2.0	Cheonan	CN	41.5	46.5	1.8	Incheon*	IC	58.7	32.7	1.5
Gangneung	GN	62.5	29.1	2.0	Cheongju	CJ	48.3	41.7	1.3	Seoul*	SU	51.8	38.2	3.8
Gunsan	GS	52.3	34.2	2.7	Daegu*	DG	50.4	41.3	1.6	Suwon	SW	42.0	49.4	1.8
Jeju	JJ1	53.8	29.2	4.3	Daejeon*	DJ	49.2	40.5	1.5					
Mokpo	MP	46.1	30.9	8.5	Gumi	GM	48.2	42.0	2.7					
Pohang	PH	53.9	34.4	4.1	Gwangju*	GJ	41.5	41.3	4.8					
Seosan	SS	45.1	35.6	5.3	Jecheon	JC	50.8	38.6	4.0					
Ulsan*	US	55.5	32.1	2.5	Jeonju	JJ2	47.4	36.1	4.2					
Yeosu	YS	52.2	34.1	4.3	Jinju	JJ3	55.5	29.2	6.2					
					Wonju	WJ	39.5	50.8	2.3					
Coastal averages		53.1	32.8	3.8	Inland averages		45.9	41.9	3.1	SMA averages		52.2	38.3	2.6
Nationwide averages		49.8	37.7	3.3										

* : Major metropolitan cities in South Korea

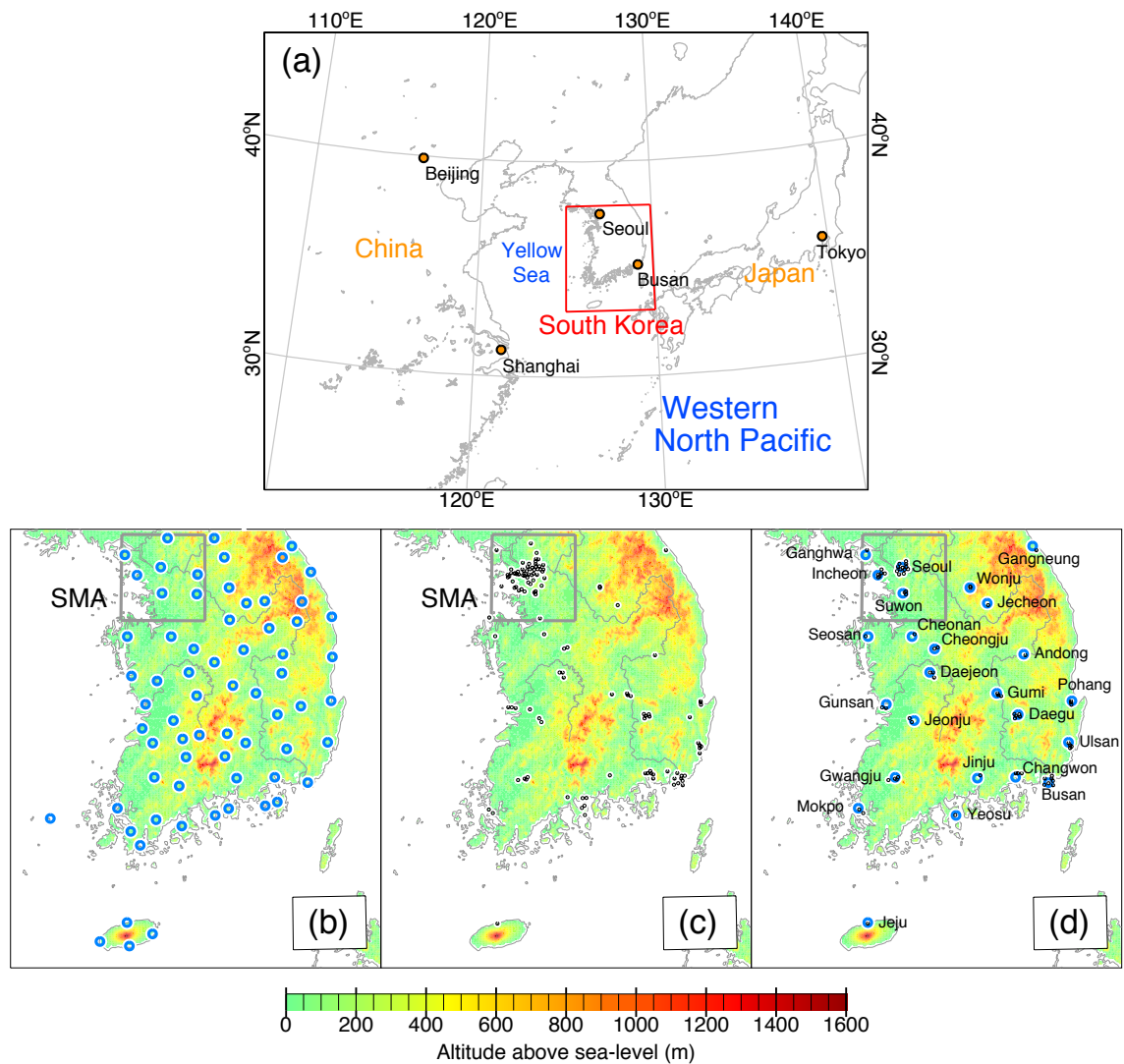


Figure 1. (a) Geographical locations of South Korea, and (b) 72 weather stations of the Korea Meteorological Administration (KMA) with blue circles, (c) 124 air quality monitoring sites of the National Institute of Environmental Research (NIER) with black dots, and (d) 72 air quality monitoring sites of NIER, which are located within 10 km from 25 weather stations of KMA over the South Korean domain.

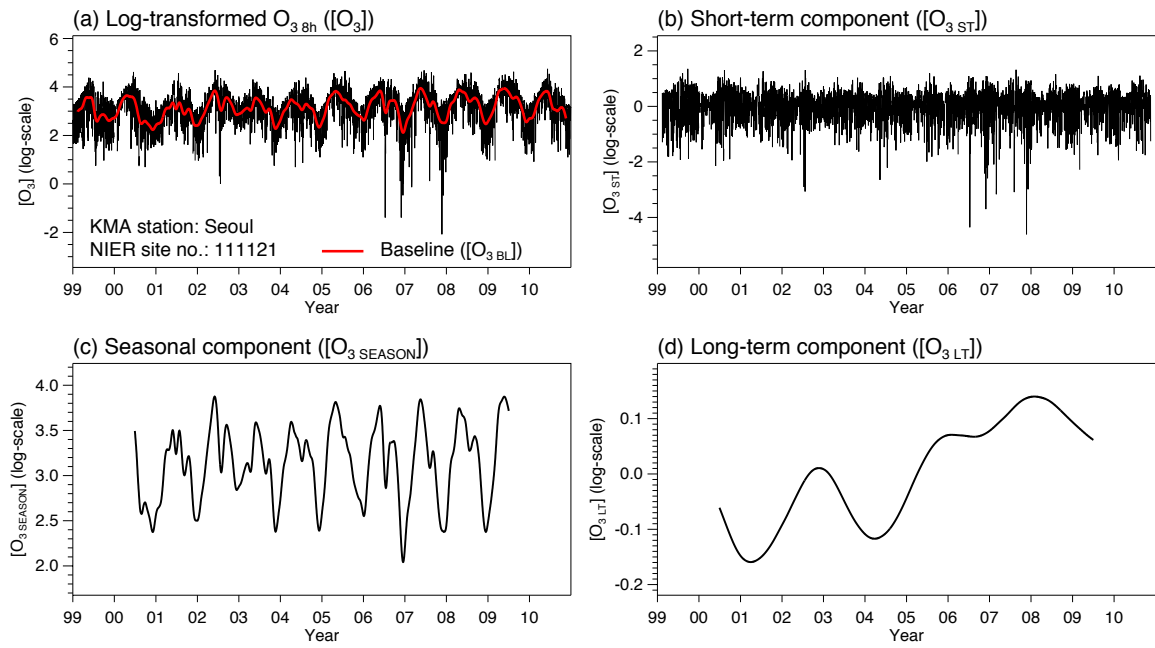


Figure 2. Time series of daily maximum 8-h average ozone (O_{3_8h}) at the City Hall of Seoul and its separated components such as (a) log-transformed O_{3_8h} time series ($[O_3]$) and its baseline ($[O_{3_BL}]$), (b) short-term component ($[O_{3_ST}]$), (c) seasonal component ($[O_{3_SEASON}]$), and (d) long-term component ($[O_{3_LT}]$) by applying KZ-filter. It is noted that the longer window length causes the larger truncation of the result (Wise and Comrie, 2005) since the KZ-filter is an iterative moving average process. The baseline in red solid line is superimposed in (a).

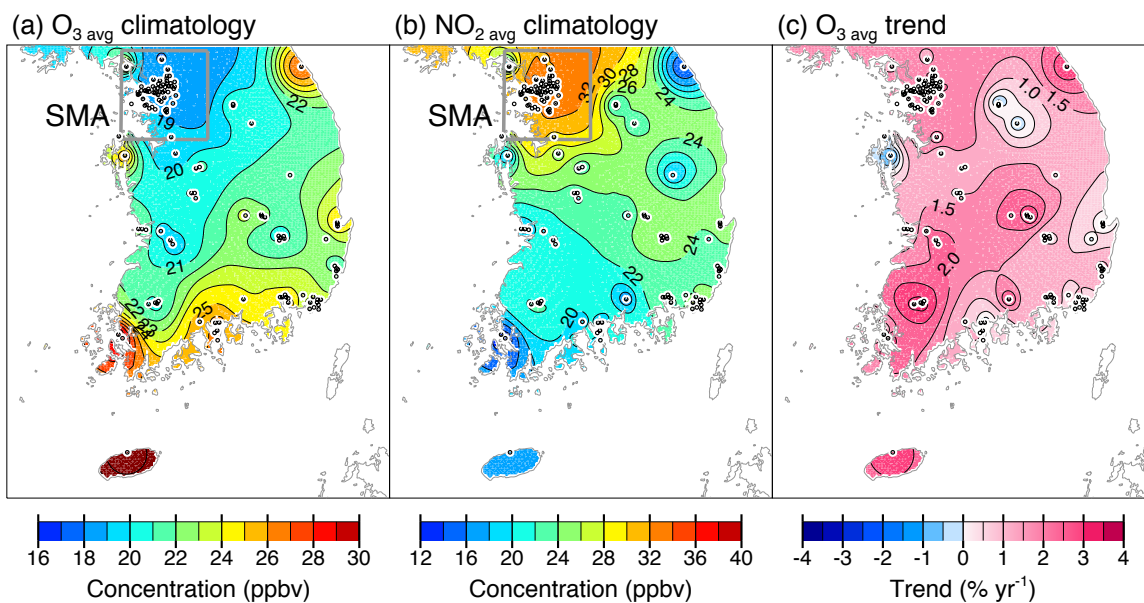


Figure 3. Spatial distributions of 12-yr averaged concentrations of (a) daily average O_3 ($O_{3\text{ avg}}$) and (b) daily average nitrogen dioxide ($NO_{2\text{ avg}}$), and (c) temporal linear trends of $O_{3\text{ avg}}$ for the period 1999–2010 using data from 124 air quality monitoring sites (black dots) of NIER.

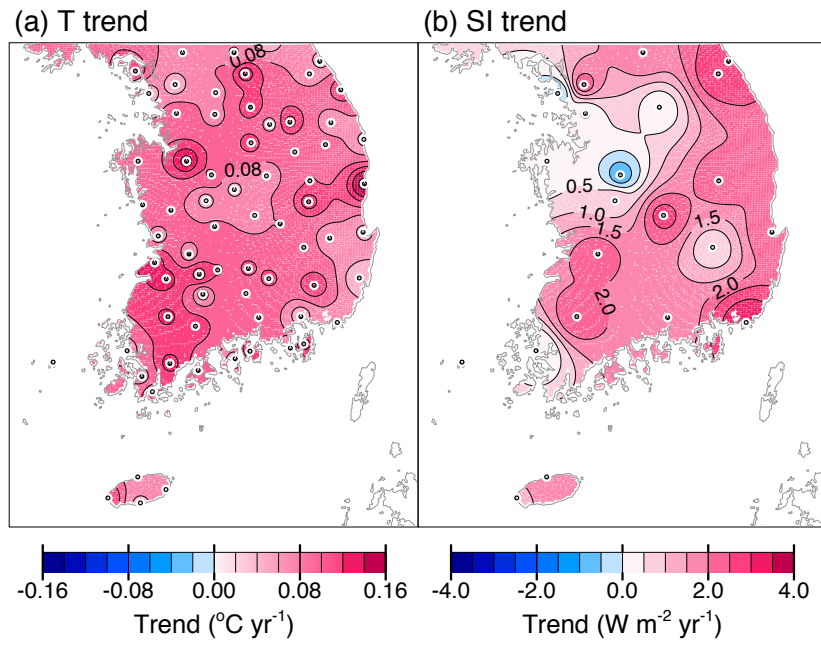


Figure 4. Spatial distributions of temporal linear trends of (a) daily average temperature (T) and (b) daily average surface insolation (SI) for the period 1999–2010 using data from 72 and 22 weather stations (black dots) of KMA, respectively.

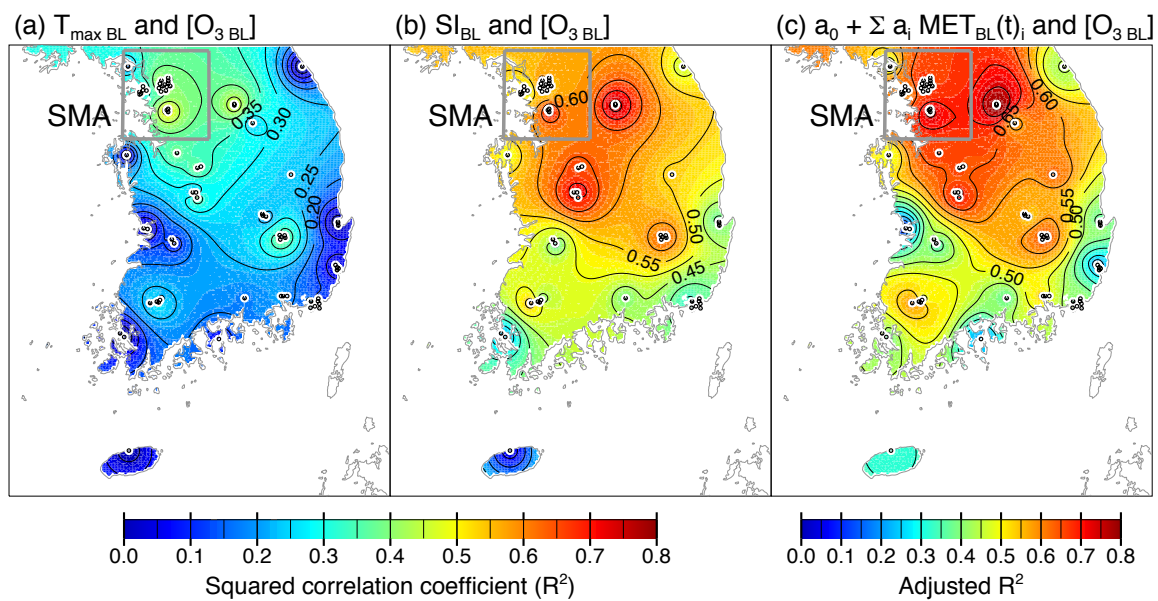


Figure 5. Spatial distributions of squared correlation coefficients (R^2) between baselines of O_3 $8h$ ($[O_3 BL]$) and (a) daily maximum temperature ($T_{\max BL}$) and (b) surface insolation (SI_{BL}). Black dots represent 72 air quality monitoring sites of NIER. (c) Spatial distribution of adjusted R^2 between $[O_3 BL]$ and combined meteorological effects ($a_0 + \sum_i a_i MET_{BL}(t)_i$).

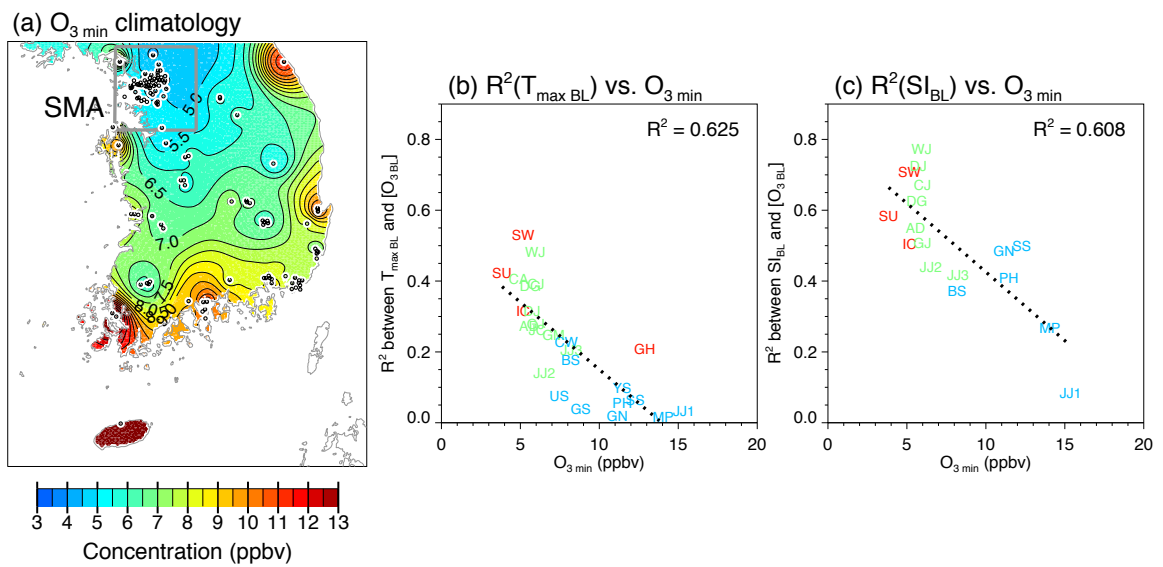
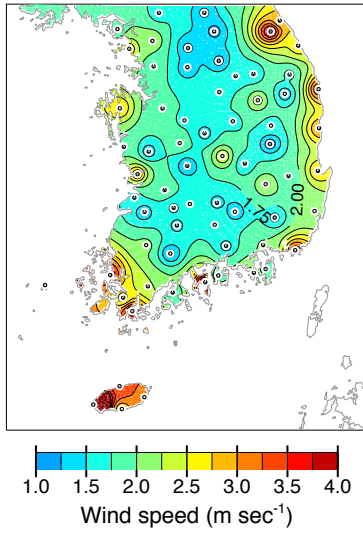
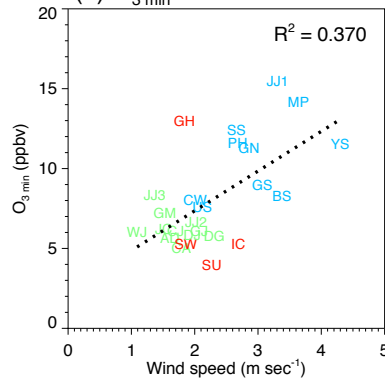


Figure 6. (a) Spatial distribution of 12-yr averaged concentrations of daily minimum O_3 ($O_{3 \min}$) for the period 1999–2010 using data from 124 air quality monitoring sites (black dots) of NIER. (b) Scatter plot of R^2 between $[O_{3 \text{BL}}]$ and $T_{\max \text{BL}}$ versus $O_{3 \min}$ at 25 cities. (c) Scatter plot of R^2 between $[O_{3 \text{BL}}]$ and SI_{BL} versus $O_{3 \min}$ at 17 cities. City codes in red, green, and blue indicate the Seoul Metropolitan Area (SMA), inland, and coastal cities, respectively.

(a) WS climatology



(b) O_3 min vs. WS



(c) $R^2(T_{\max BL})$ vs. WS

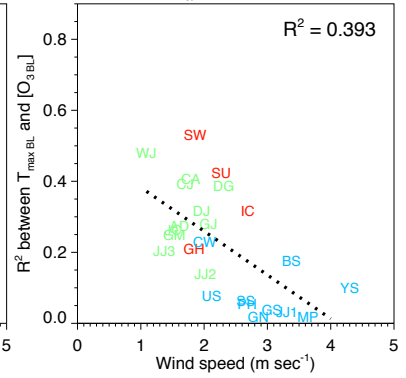


Figure 7. (a) Spatial distribution of 12-yr averaged daily average wind speeds (WS) for the period 1999–2010 using data from 72 weather stations (black dots) of KMA. (b) Scatter plot of O_3 min versus WS at 25 cities. (c) Scatter plot of R^2 between $[O_3 BL]$ and $T_{\max BL}$ versus WS at 25 cities. City codes in red, green, and blue indicate the Seoul Metropolitan Area (SMA), inland, and coastal cities, respectively.

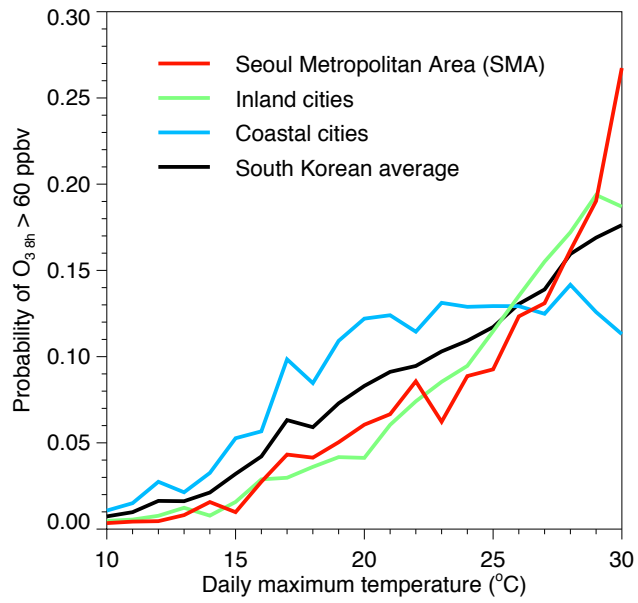


Figure 8. Probabilities of O_3 exceedances in the given range of daily maximum temperature (T_{max}) that O_3_{8h} will exceed air quality standard of South Korea (60 ppbv).

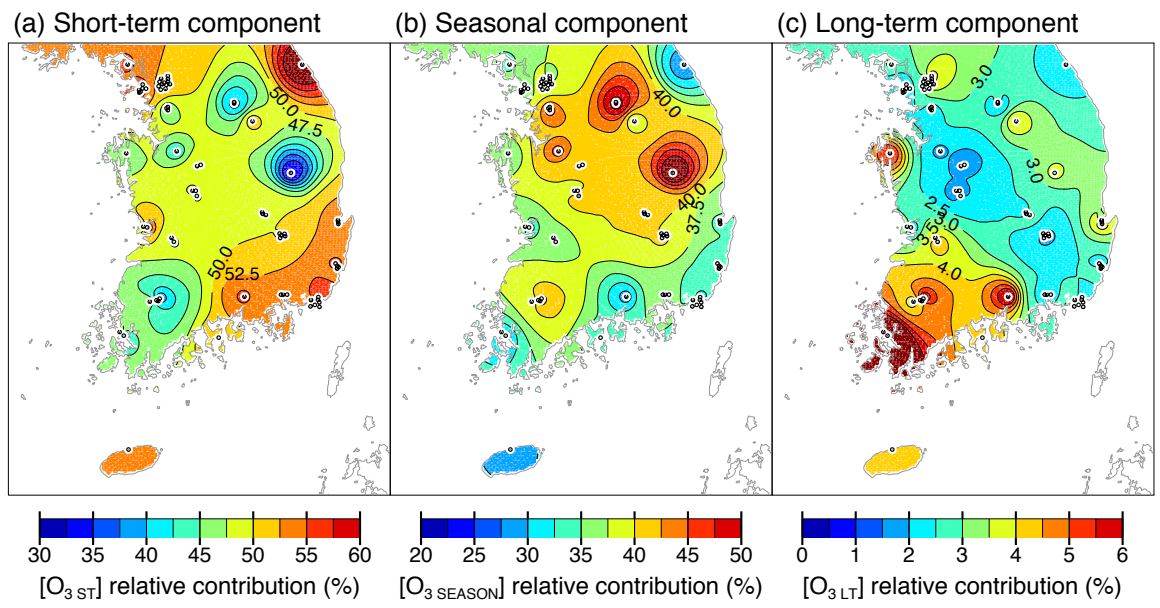


Figure 9. Spatial distributions of relative contributions of (a) short-term component ($[O_3_{ST}]$), (b) seasonal component ($[O_3_{SEASON}]$), and (c) long-term component ($[O_3_{LT}]$) to the total variance of original time series ($[O_3]$) using data from 72 air quality monitoring sites (black dots) of NIER. Note that the color scales are all different.

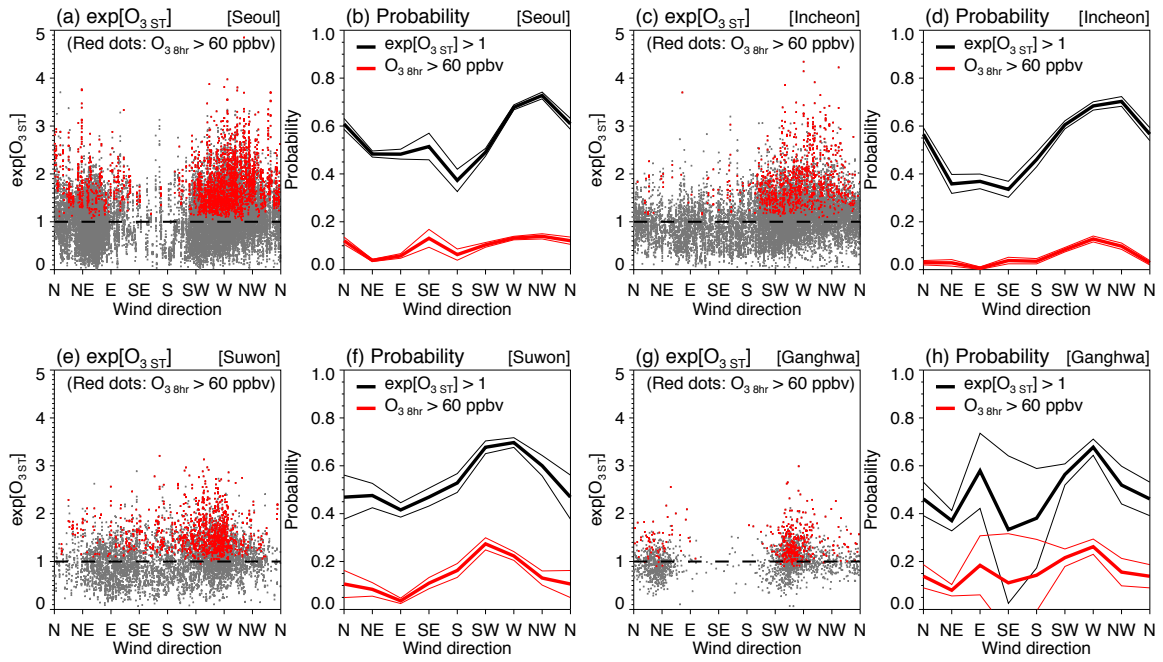


Figure 10. Relationships between wind directions (WD) and exponentials of short-term components ($\exp[\text{O}_3_{\text{ST}}]$) during the months of frequent high O_3 events (May–October) at Seoul (a–b), Incheon (c–d), Suwon (e–f), and Ganghwa (g–h) in the Seoul Metropolitan Area (SMA) are represented in scatter plots of $\exp[\text{O}_3_{\text{ST}}]$ versus WD (a, c, e, and g) and probabilities of O_3 exceedances in each WD (b, d, f, and h). Red dots in scatter plots denote high O_3 episodes that daily maximum 8-h average O_3 ($\text{O}_3_{8\text{h}}$) will exceed air quality standard of South Korea (60 ppbv). Dashed lines in scatter plots denote the reference of $\exp[\text{O}_3_{\text{ST}}] = 1$. Probabilities of $\exp[\text{O}_3_{\text{ST}}] > 1$ and $\text{O}_3_{8\text{h}} > 60$ ppbv in each WD are represented as black thick lines and red thick lines, respectively. 95% of confidence intervals for each probability are represented as black and red thin lines. We used O_3 data from 12 sites in Seoul, 6 sites in Incheon, 3 sites in Suwon, and 1 site in Ganghwa.

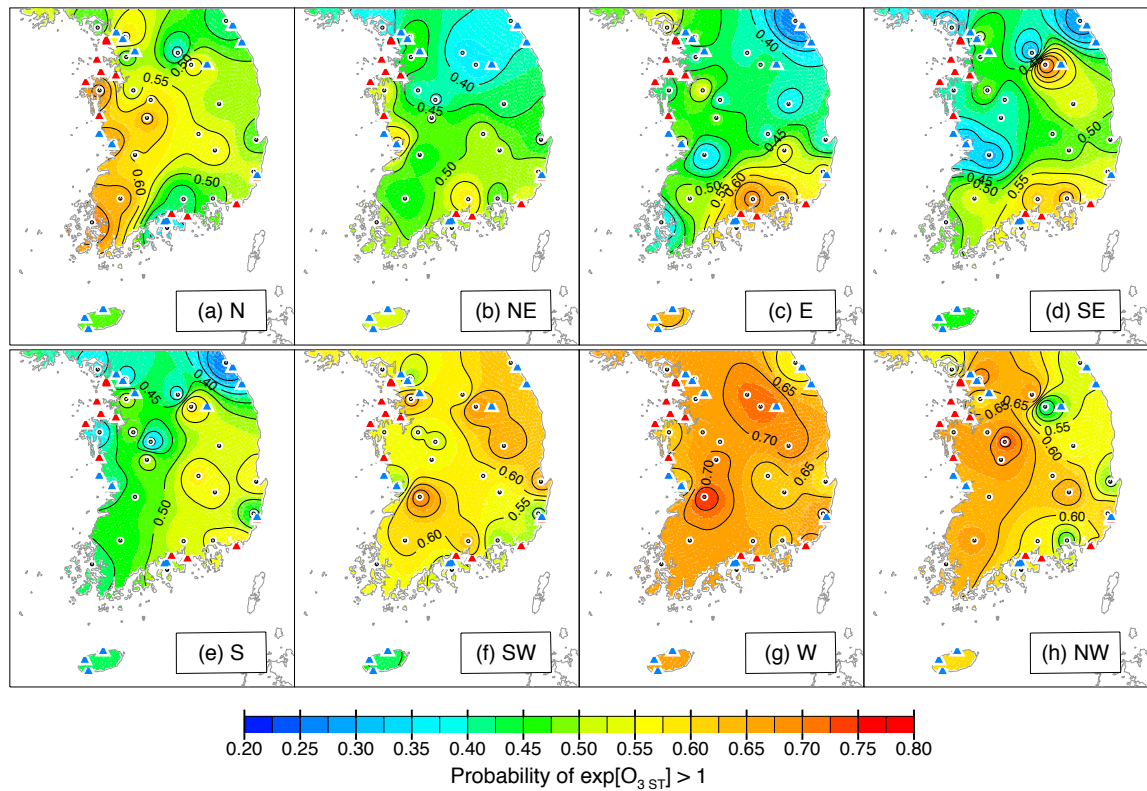


Figure 11. Spatial distributions of probabilities that exponentials of the short-term components will exceed 1 ($\exp[O_{3_ST}] > 1$) for each wind direction (WD) of (a) northerly (N), (b) northeasterly (NE), (c) easterly (E), (d) southeasterly (SE), (e) southerly (S), (f) southwesterly (SW), (g) westerly (W), and (h) northwesterly (NW), respectively. Black dots denote 25 weather stations of KMA and triangles denote 26 major thermoelectric power plants in South Korea (blue triangle < 1000 MW, red triangles ≥ 1000 MW).

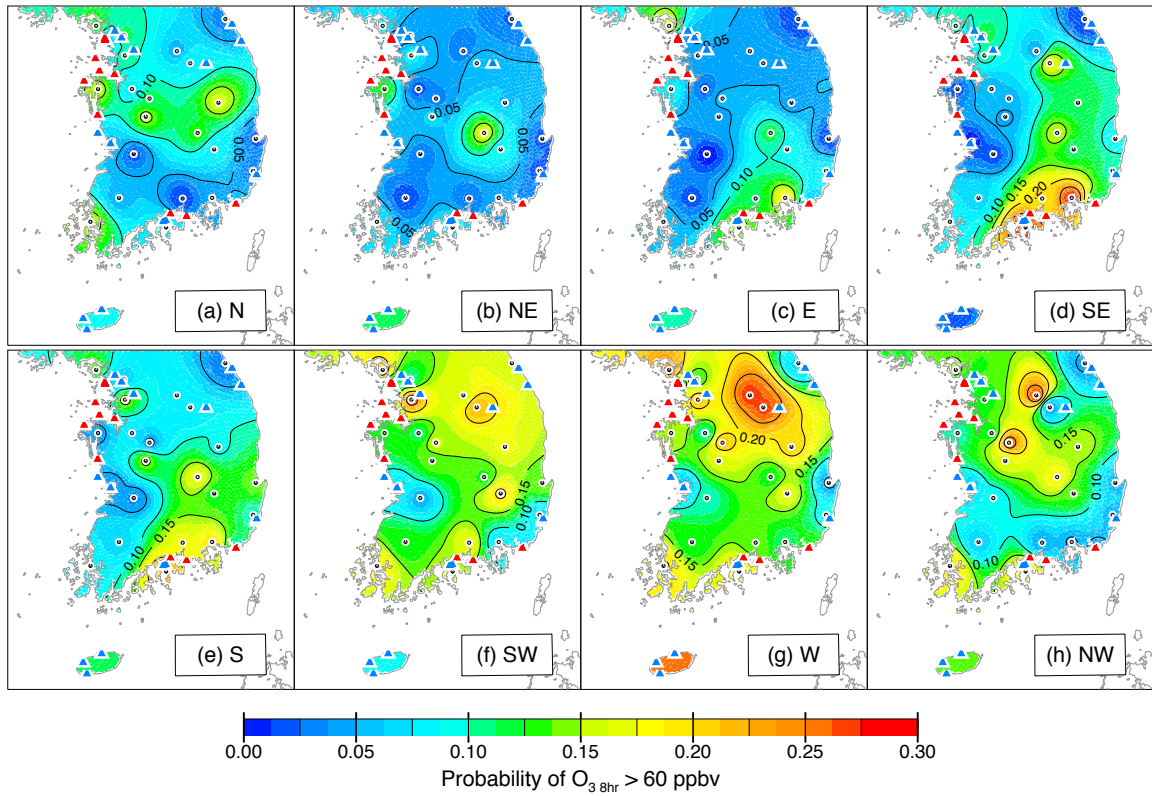


Figure 12. Spatial distributions of probabilities that daily maximum 8-h average O_3 ($O_{3_{8h}}$) will exceed air quality standard of South Korea (60 ppbv) for each wind direction (WD) of (a) northerly (N), (b) northeasterly (NE), (c) easterly (E), (d) southeasterly (SE), (e) southerly (S), (f) southwesterly (SW), (g) westerly (W), and (h) northwesterly (NW), respectively. Black dots denote 25 weather stations of KMA and triangles denote 26 major thermoelectric power plants in South Korea (blue triangle < 1000 MW, red triangles \geq 1000 MW).

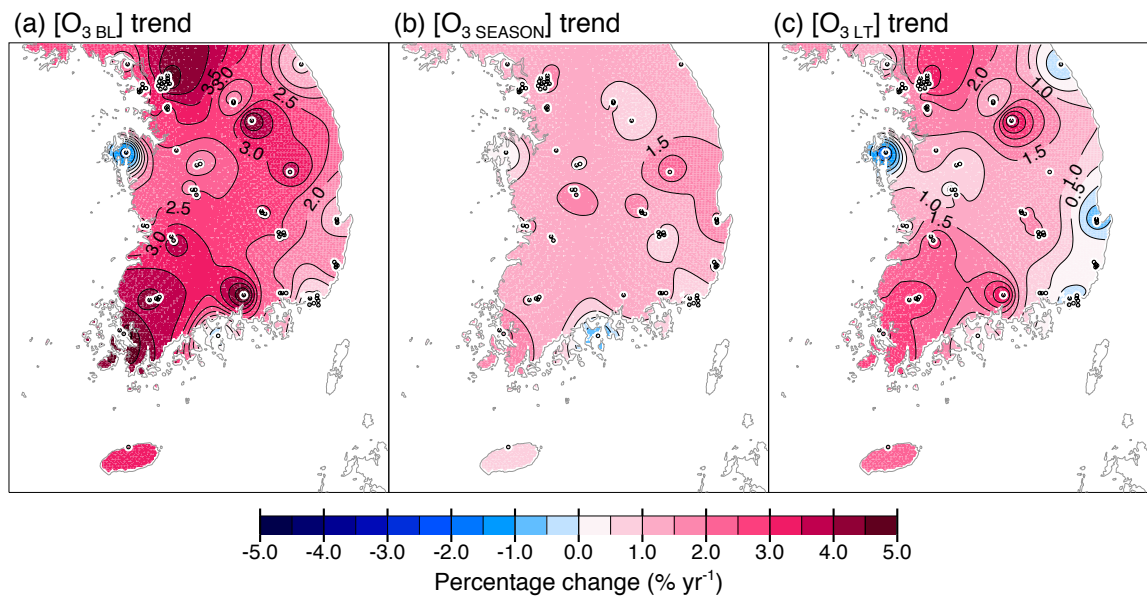


Figure 13. Spatial distributions of temporal linear trends of (a) baseline ($[O_3_{BL}]$), (b) seasonal component ($[O_3_{SEASON}]$), and (c) long-term component ($[O_3_{LT}]$) for the period 2000–2009 using data from 72 air quality monitoring sites of NIER.

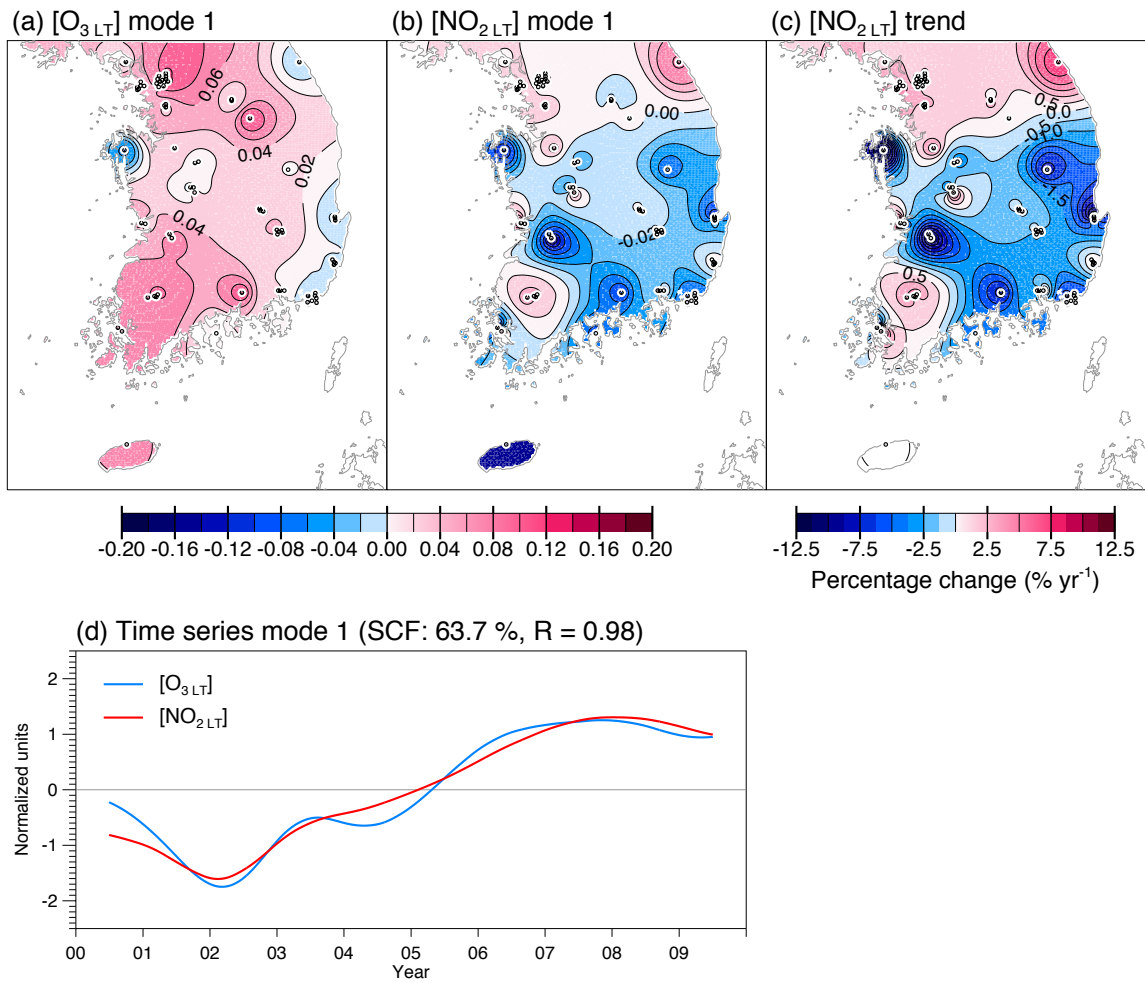


Figure 14. The first leading mode of SVD between the long-term components of (a) daily maximum 8-h average O_3 ($[O_{3\text{LT}}]$) and (b) daily average NO_2 ($[NO_{2\text{LT}}]$) for the period 2000–2009. (c) Spatial distribution of temporal linear trends of $[NO_{2\text{LT}}]$. (d) Time series of the SVD expansion coefficient associated with $[O_{3\text{LT}}]$ mode (blue line) and $[NO_{2\text{LT}}]$ mode (red line).